TECHNICKÁ UNIVERZITA V LIBERCI
Fakulta strojní

Heat transfer in technological processes

Diplomová práce

Studijní program: N2301 – Mechanical Engineering
Studijní obor: 2302T010 – Machines and Equipment Design

Autor práce: **Shkurte Kastrati**
Vedoucí práce: doc. Ing. Tomáš Vít, Ph.D.

Liberec 2016

TECHNICAL UNIVERSITY OF LIBEREC
Faculty of Mechanical Engineering

Heat transfer in technological processes

Diploma thesis

Study programme: N2301 – Mechanical Engineering
Study branch: 2302T010 – Machines and Equipment Design

Author: **Shkurte Kastrati**
Supervisor: doc. Ing. Tomáš Vít, Ph.D.

Liberec 2016

Technical University of Liberec
Faculty of Mechanical Engineering
Academic year: **2015/2016**

DIPLOMA THESIS ASSIGNMENT

(PROJECT, ART WORK, ART PERFORMANCE)

First name and surname:	**Shkurte Kastrati**
Study program:	**N2301 Mechanical Engineering**
Identification number:	**S15000594**
Specialization:	**Machine and Equipment Design**
Topic name:	**Heat transfer in technological processes**
Assigning department:	**Department of Power Engineering Equipment**

Rules for elaboration:

Manufacturing of ultra-precise optics (especially the lightweighted structures) deals with a number of specific problems, which are connected to stiffness of the structures, material properties and by influence of the temperature and heat transfer processes. The objective of the thesis is to describe in details the process of bonding of the glass (or optical ceramics) on CNC holders. The aim of you work will be to perform numerical simulation of bonding and consecutive manufacturing (grinding) of precise optics.

Thesis structure:

1. Literature overview.
2. Overview of theory of precise optics manufacturing process.
3. Overview of material properties and material models.
4. Development of the Method for evaluation of the results.
5. Numerical simulation of the manufacturing process.
6. Design of experiments.
7. Shape measurement and surface quality measurement.
8. Comparison of the results from simulations and experiments.

Scope of graphic works:	**20 pages**
Scope of work report (scope of dissertation):	**45 pages**
Form of dissertation elaboration:	**printed**
Language of dissertation elaboration:	**English**

List of specialized literature:

[1] **ASKIN, G., STANDRIDGE, R. 1993.** *Modeling and Analysis of Manufacturing Systems.* **John Wiley, New York.**

[2] **MALACARA, D. Malacara. 2001.** *Handbook of Optical Engineering.* **CRC Press.**

[3] **DRIGGERS, R. G.. 2003.** *Encyclopedia of Optical Engineering.* **CRC Press.**

Tutor for dissertation:	**doc. Ing. Tomáš Vít, Ph.D.** Department of Power Engineering Equipment
Date of dissertation assignment:	**18 November 2015**
Date of dissertation submission:	**18 February 2017**

prof. Dr. Ing. Petr Lenfeld
Dean

Technická univerzita v Liberci - 7a -

doc. Ing. Václav Dvořák, Ph.D.
Head of Department

Liberec, dated: 18 November 2015

Prohlášení

Byla jsem seznámena s tím, že na mou diplomovou práci se plně vztahuje zákon č. 121/2000 Sb., o právu autorském, zejména § 60 – školní dílo.

Beru na vědomí, že Technická univerzita v Liberci (TUL) nezasahuje do mých autorských práv užitím mé diplomové práce pro vnitřní potřebu TUL.

Užiji-li diplomovou práci nebo poskytnu-li licenci k jejímu využití, jsem si vědoma povinnosti informovat o této skutečnosti TUL; v tomto případě má TUL právo ode mne požadovat úhradu nákladů, které vynaložila na vytvoření díla, až do jejich skutečné výše.

Diplomovou práci jsem vypracovala samostatně s použitím uvedené literatury a na základě konzultací s vedoucím mé diplomové práce a konzultantem.

Současně čestně prohlašuji, že tištěná verze práce se shoduje s elektronickou verzí, vloženou do IS STAG.

Datum: 27. 05. 2016

Podpis: 

Annotation

The objective of this thesis is to describe in details the process of bonding of ZERODUR mirrors on CNC holder, and the influence of the heating and cooling of the wax on the final shape of mirror. For bonding of the ZERODUR glass to the aluminum holder we have used red wax, and we have monitor the influence of this material to the final shape of our optic by measuring the surface shape before and after bonding by using the LuphoScan. Furthermore the consecutive process of bonding numerically is verified by using MSC Marc& MSC Mentat 2015. This work shows that for manufacturing of ultra-precise optics bonding of the ZERODUR glass to the ZERODUR disk gives better results, compared to aluminum disk.

Keywords: visco- elastic, precision machining, grinding, polishing, heat transfer, experiments, FEM

Table of Contents

List of Tables

List of Figures

List of Symbols

z	$[1]$	Saggita error
R	$[m]$	paraxial surface radius
R_e	$[1]$	Reynold's number
ρ	$[kg \cdot m^{-3}]$	Density
v_{slot}	$[m \cdot s^{-1}]$	Coolant velocity
h_{slot}	$[mm]$	Slot thickness
D	$[m]$	Diameter
Q_w	$[mm^3 \cdot s^{-1}]$	Material removal rate
a_e	$[mm]$	Depth of cut
f_r	$[mm \cdot rev^{-1}]$	Feed per revolution
v_w	$[mm \cdot s^{-1}]$	Workpiece surface speed
R_c	$[mm]$	Grinding wheel cutting radius
z_c	$[\mu m]$	Controlled depth
z_t	$[1]$	Grinding wheel direction
F_t	$[N]$	Tangential grinding force
P_c	$[W]$	Grinding power
v_d	$[1]$	Abbe number
n_d	$[1]$	Refractive index
k	$[W \cdot m^{-1}K^{-1}]$	Thermal conductivity
c_p	$[J \cdot kg^{-1}K^{-1}]$	Specific heat capacity
E	$[Mpa]$	Young's modulus
μ	$[1]$	Poisson's ratio
α	$[K^{-1}]$	Coefficient of linear thermal expansion
G	$[MPa]$	Shear modulus
K	$[N \cdot m^{-1}]$	Stiffness
u	$[mm]$	Nodal displacement

List of Abbreviations

Å	Angstrem
Al	Aluminum
CTE	Coefficient of linear Thermal Expansion
METIS	Multi Element Telescope for Imaging and Spectroscopy
ESA	European Space Agency
IEO	Inverted External Occulter
SL	Solar Disk Light
UV	Ultra Violet
VIS	Visible channel
LS	Layout Stop
IO	Internal Occulter
NASA	National Aeronautics and Space Administration
ISO	International Organization for Standardization
CNC	Computer Numerical Control
EUVL	Extreme Ultra Violet Lithography
RMS	Root Mean Square
SPDT	Single Point Diamond Turning
FAG/LAG	Fixed/Loose Abrasive Grinding
IBF	Ion Beam Figuring
BK7	Bor-crown glass
ANSI	American National Standards Institute
FEPA	Federation Europeenne des fabricants de Produits Abrasifs
RAP	Reactive Atom Plasma
CCP	Computer Controlled Polishing
MRF	Magneto Rehological Finishing
ULE	Ultra- Low Expansion
FJP	Fluid Jet Polishing
SiC	Silicon Carbide
GTC	Gran Telescopio Canarias

TOPTEC	Turnov OPToElectronic Centre
RTV	Room Temperature Vulcanization
CVD SiC	Chemical Vapor Deposition Silicon Carbide
SSD	Sub Surface Damage
Adv.	Advantages
Disadv.	Disadvantages
M1	Mirror 1
M2	Mirror 2
SSiC	Sintered Silicon Carbide
ULE	Ultra- Low Expansion
BK7	Bor-Crown Glass
SiSiC	Silicon infiltrated Silicon Carbide
MWLI	Multi Wavelength Interferometry
PV	Peak to valley

Acknowledgements

I would like to express my gratitude to my supervisor Doc. Ing. Tomáš Vít, not only for his help, advice, and consultations about thesis, but also for the help he offered me in completing my studies at Technical University of Liberec.

I would like to thank the Centre of Special Optics and Optoelectronics- TOPTEC, for giving me the chance to contribute in this project.

I would like to thank also the staff and my friends at Faculty of Mechanical Engineering. A special thank goes to Marcela Válková for offering me her help and advice whenever I asked for.

Profound thanks go always to my family, whose help and support made always everything possible.

Respectfully,

Shkurte Kastrati

Dedicated to my parents, Mehmet and Mevlide Kastrati, and my sibilings Havishe, Arijeta and Egzon Kastrati

Chapter 1: Introduction

Manufacturing of ultra- precise optics deals with a number of specific problems which are connected to stiffness of the structure, material properties, by influence of temperature, and heat transfer processes.

Most optical fabrication processes begin with the extremely important consideration of holding onto part during subsequent fabrication steps. So, motivation behind this work is to demonstrate the process of bonding of Zerodur glass into CNC holder. As a holder in our case we have chosen it to be made from aluminum (brass) with rigidity being the most important factor, over it to be cemented either a Zerodur disk or aluminum disk, for which we have performed the numerical simulation in MSC Marc and made the comparison in using one or another. For gluing mirror over the disk we have used red wax as adhesive, and ceramic glass of Zerodur as our optic that has to be bounded and after it undergo the manufacturing process.

In general, “precise’’ optics is used in literature as a term for the optical parts with very low surface roughness, very high form accuracy and high surface integrity.

Precision optics are essential to orbiting space telescopes as they reveal the outer reaches of the surrounding Universe. Modern telescopes for space applications use complex optical elements like aspheres or freeforms, so the requirements for precise optics are still increasing.

Demand for maximum loss weight goes together with demands for sufficient strength, shape accuracy and surface quality of optical surfaces. These requirements not only stem from space research, but also from applications that require fast and accurate mirror position changes, such as military optics or scanning optics. Lightweight mirrors are usually made by modifying the geometry of the substrate. A special structure in the form of ribs or honeycombs must be designed to ensure sufficient response to the planned loads. An example of a lightweight spherical mirror is shown in fig. 1.

Figure 1: Example of spherical mirror from SiSiC and lightweight base plate structure [22]

Optical glass and optical ceramics (e.g. Zerodur), which are usually supplied in crude block or disk form, are frequently used as a substrate material for manufacturing lightweight mirrors. However these materials present significant disadvantage in the production of lightweight optical elements. The machining of silica glass and ceramics, which are extremely brittle must be carried out at very low speeds to prevent subsurface damage and deep fracture. The limiting factor for machining speed is also origination of residual stresses in the structure. The manufacturing of optical glass and ceramics which results in complex lightweight structures, takes several working days or even weeks. [22]

ESA mission of Solar Orbiter dedicated to solar and heliospheric investigation, namely to explore the Sun will be launched in October 2018. The Multi Element Telescope for Imaging and Spectroscopy METIS is one of the ten instruments allocated in the Solar Orbiter.

Centre TOPTEC is responsible for manufacturing of two main mirrors of METIS telescope. METIS telescope is an inverted external occulter solar cornograph for VIS and UV imaging.

A potential application of our work is to show how much the process of heat transfer during manufacturing, especially during grinding of mirrors influences the final shape of METIS aspherical Zerodur mirrors.

Chapter 2: Literature review

Now days the range of objective shapes being used in high technology optical systems has become more diverse. Precision optical systems comprising purely spherical and planar elements are becoming less common. The reasons behind the move toward more complex shape optics are concerned with producing smaller, lighter and generally less complicated systems in regard to the number of elements. Quality aspects can also be attained with these more complex elements.
The use of aspherical shape objectives to reduce spherical aberration permits a reduction of the number of elements required in a given system and is becoming a more common practice. [1]

Modern trends in the field of optical components fabrication require more space efficient and more lightweight optical systems, which cannot be often realized by common spherical optics and aspherical or even freeform optics must be used. In fabrication of aspherical optics the particular aim is to reach the required accuracy of polished element in the shortest possible amount of time. Therefore it is necessary to reach a very high precision of the element shape before the beginning of the polishing process itself. To reach that an iterative way of grinding have to be used. Firstly, the element is grinded and measured and in the following step (or further steps), the measured data serve as a feedback for the grinding machine to correct the deviations from the nominal shape. Rather accurate and fast measurement method for grinded surface form is therefore an inseparable part of the fabrication chain not only for final figuring and inspection. [2]

A recent lithography technique, Extreme Ultraviolet Lithography EUVL, has imaging beams reflected by mirrors instead of refracted by lenses. [3] It requires projection optics with a figure accuracy of 0.25 nm rms. The roughness levels are 0.20 nm rms mid-spatial frequency roughness and high spatial frequency roughness of 0.10 nm rms. These optics needs to be aspherics.

The lithography masks are made of low CTE optics materials such as Zerodur, BK7 and ULE. The PV accuracy needs to be better than 50 nm. Low defects concentration is also required. [4]

METIS- the Multi Element Telescope for Imaging and Spectroscopy for the ESA Solar Orbiter, the target of which is the solar corona from a near-Sun orbit is made of aspherical Zerodur mirror. METIS adopts a novel inverted externally occulted configuration, where the disk light is shielded by an annular occulter, and an annular aspherical mirror M1 collects the signal coming from the corona. After M1 the coronal light passes through an internal occulter and is then reflected by a second annular mirror M2 toward a narrow filter for the 121.6 nm HI line selection. [6]

In figure 2 is shown METIS telescope allocated in Sorlar Orbiter.

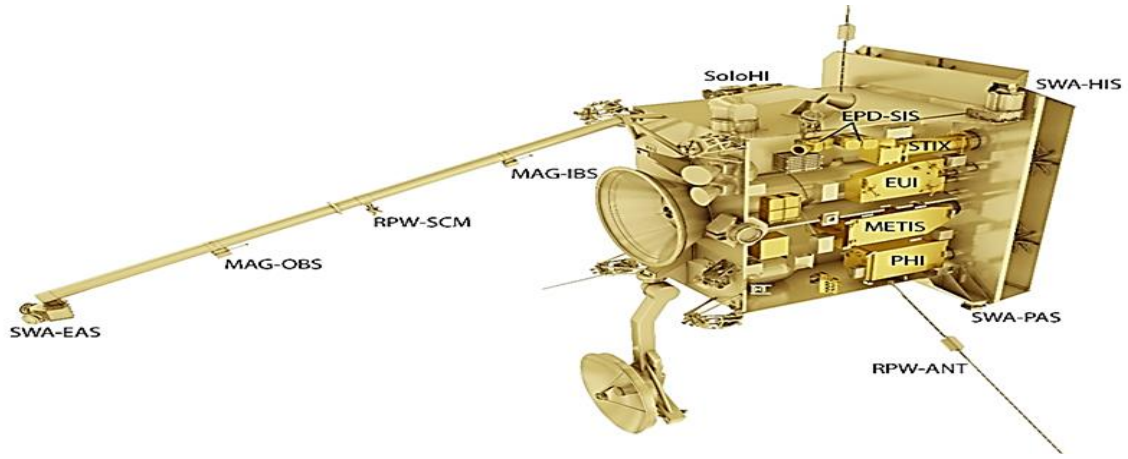

Figure 2: Payload accommodation on board Solar Orbiter.

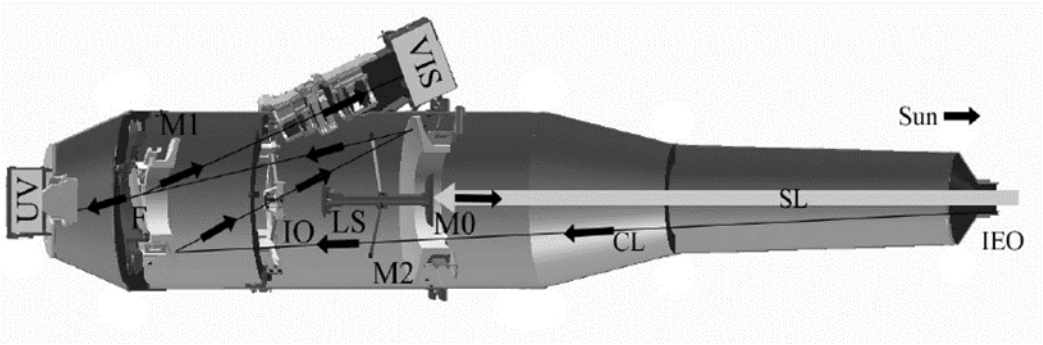

Figure 3: Optomechanic structure of METIS. [6]

In figure 3 is shown the optmechanic strucutre of METIS.

Technical challenges for METIS: Very precise shaping of the occulting elements: edge curvature radius < 50 μm, and extreme polishing of the mirror surfaces: roughness = 0.3 nm rms (0.2 nm goal). [8]

The surface micro-roughness (2 Å for M1 and 3 Å for M2) and shape accuracy (better then l/10) is necessary for overcoming stray light, whereas the stiffness and weight of the mirrors is important for keeping the mass budget low. The total weight of both mirrors is required to be less than 1 kg.[23]

Large optics (> 50 cm) are almost always mirrors, and have other unique difficulties due to their size and surface requirements. For the same optical performance, a mirror surface must be

four times better than a refractive surface. The support for large optics becomes difficult and extremely sensitive. Often, separate supports must be used for holding the optics during polishing than can be used for testing. The polishing forces from large laps can be substantial and must be resisted by the support. The self-weight deflection of large mirrors alone will quickly dominate the shape if it is not accommodated in the support. It is much more difficult to estimate the costs for large optics than for small ones because of the difficulties with large optics and the fact that each one is special. A different issue is the choice of substrate material for reflective optics. The light does not care what substrate the mirror is made of because it reflects off a coating on the surface and never goes through the mirror. The mirror substrate can be chosen according to the operating environment. Frequently, mirrors are made from low expansion glass because this takes an excellent polish, and it minimizes the sensitivity to thermal effects. Mirror substrates can be procured as light-weighted structures to reduce the self-weight deformation. [18]

By 2030, NASA roadmap on precise optics shows demands for a decrease in areal density and cost by two and ten times respectively. [9]

.

2.1 Definition of Aspherical Optical Elements

Aspherical optical surfaces deviate more or less pronouncedly from the spherical shape of standard optical surfaces. They are used in optical systems to increase imaging quality, to reduce construction size or the number of elements, to save weight, to simplify the assembly process, or to reduce the overall manufacturing costs.

Aspherical optical elements can be produced in several configurations: as one aspherical surface on a substrate (e.g., a parabolic reflector), as a combination of aspherical surfaces with spherical surfaces (e.g., aspherical lenses) or as a combination of several aspherical surfaces (e.g., bi-aspheric lenses, free shaped prisms).

Aspherical surfaces can be described by continuous mathematical functions. They can be rotationally symmetric, axially symmetric, or completely asymmetric (free- form surfaces).

Dependent on the production volume, on the degree of asphericity, and on the required tolerance values aspherical elements can be manufactured by a variety of production methods, for example by casting and injection molding of plastics, by blank pressing of glass, or by precise

machining (diamond turning of metals or polymers, grinding and polishing of metals, optical glasses, crystals, ceramics) .

2.2 Basic characteristics of aspherical elements compared with spherical elements

2.2.1 Quality of the surface form

Spherical surfaces are characterized by a constant curvature value and thus can be manufactured using large format tools. These tools are state of the art and operate, when properly driven, over a long period of time without significant quality degradations. Additionally, the tooling heads move in a rather stochastical way, which avoids the generation of "zonal" artifacts in the surface structure. Consequently, very high form accuracies can be achieved, even with relatively simple machines.

In the case of aspheres, the local curvature changes across the surface requiring small tooling heads for grinding and polishing. These tools are more sensitive to the deteriorations that destabilize the process. Very accurate machine kinematics and complex corrections procedures are required, and the risk of generating artifacts is rather large. Additionally very precise measuring methods with accuracies in the range 500 nm to below 1 nm are indispensable. Because several correction loops must often be performed, artificial ripples in the surface structure cannot be avoided completely and must be carefully tolerated.

2.2.2 Quality of surface texture

The small- area working tools mentioned, in combination with deterministic tool path, with little room for stochastic movements, tend to decrease the quality of the surface texture. In order to achieve the same high degree of polishing as obtained with spherical surfaces, more technical efforts are necessary. For example, grinding must be performed with smaller grain sizes, of 10 µm down to 3 µm, and with small tool pressure, leading to long working times. The polishing times are also much longer than those needed for equivalent spherical surfaces. Recent progress in polishing technology such as, magnetorheological polishing techniques (and the appropriate

polishing fluids), which are used for finishing all kinds of optical surfaces, yields both high quality surface form and texture.

2.3 Mathematical representation of aspherical surfaces

2.3.1 Basic equation according to ISO 10110- Part 12

The standard ISO 10110 Part-12 describes surface functions of second order with axial symmetry as:

$$z = f(r) = \frac{\frac{r^2}{R}}{1 + \sqrt{1 - (1+\kappa)\left(\frac{r}{R}\right)^2}} + \sum_{n=2}^{m} A_{2n} \cdot r^{2n} \qquad (1)$$

Where r is the lateral coordinate, z the sagitta error, and R the paraxial surface radius. The conic constant κ is 0 for spheres, -1 for parabolas, < -1 for hyperbolas, between -1 and 0 for oblate, and > 0 for prolate ellipses.

2.4 Design drivers

The reduction of the number of the optical components is only one reason to insert aspheres into optical systems. Other important design drivers are:

- To increase the imaging quality (resolution, distortion), which cannot be achieved by a pure spherical design (example: deep UV lithography)
- To reduce the construction size (example: photographic zoom lenses);
- To save weight, because one asphere is perhaps lighter than a several spherical components yielding the same optical performance;
- To improve the total light transmission by reducing the number of optical elements;
- To simplify the assembly process;

All these drivers can be combined to reduce the overall manufacturing costs.

2.5 Classifications

In addition to the mathematical description, aspherical components are often classified in a pragmatic physical/ technical sense:

- As refractive, reflective or diffractive components, if the light deflection is caused by lenses, mirrors or holographic elements;
- As “conical”, “higher aspherical” or even “free-form” components, if the surface deformation is rotational invariant around the optical axis or may lack any symmetry; and
- As “on-axis” or “off-axis” components, if axially centered or decentered to the optical system axis

2.6 Generating of aspherical optics (the historical approach)

As an introduction we start with the principle of manufacturing spherical optics, which is based on the identity of the surface functions of complementary bodies, here tool and workpiece, as shown in the figure 4. The lens (1) is moved over the rotating, full- sized stiff tool (2). The tool, which is in contact with the overall surface of the lens generates a negative copy of its shape on the lens.

Using the same kind of relative movement between lens and tools, the 2D symmetry of the surface is lost for the aspheres. In this case the area of contact between a stiff tool and the workpiece is reduced to a line or even to a point contact; for example the meridional line, as an axis of symmetry can be used as a line contact.

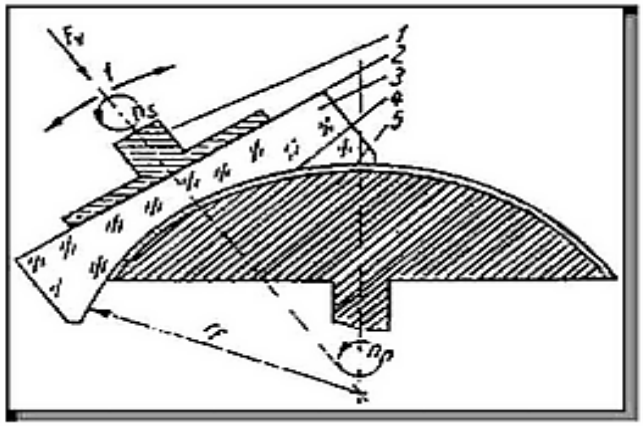

Figure 4: Principle of generating or polishing spheres using the symmetry between tool and workpiece [18]

Descartes was the first to take these considerations into account and he designed the first copying- machine where a grinding stone was used as a master. The tool (4) for generating was moved along the desired shape (6), guided by a push rod (3), but the shape accuracy was limited by insufficient guiding and bearings. Building a template of the contour line of the designed asphere, (fig. 5) was another approach for generating aspheres. The wheel (4), which is moving along the shape (6), is transferring, via a guiding system, the contour line to a grinding wheel (5) of the same size to the workpiece that has to be grounded (2). The wheel itself serves as a low-pass filter for manufacturing errors of the template.

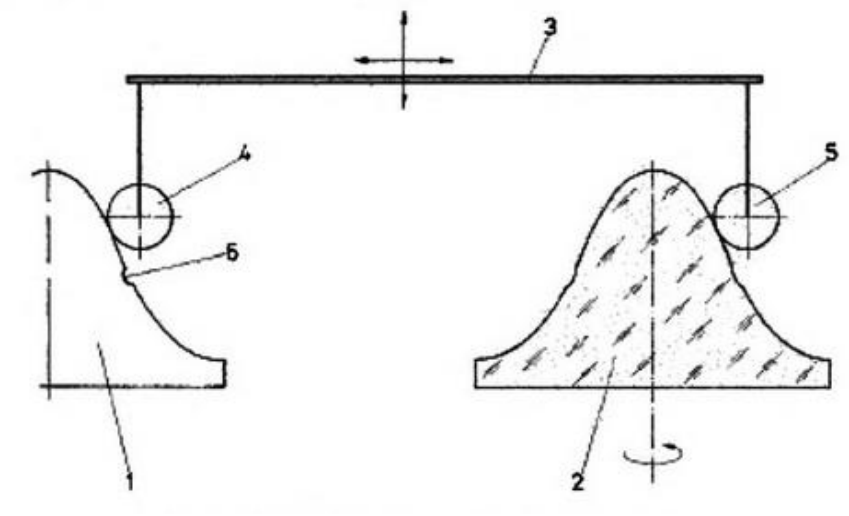

Figure 5: Principle of a copy machine for aspheres [14]

Similar to the Descarte's method, Mackenson designed and built (1920) at Zeiss a machine to manufacture aspheres. The principle of this machine is shown in fig.6. The asphere rotates (1) and has a line contact to the grinding wheel (2). The shaping tool allows permanent refiguring and is moved in an adapted polar coordinate system, which provides higher accuracy when compared to copying a simple template.

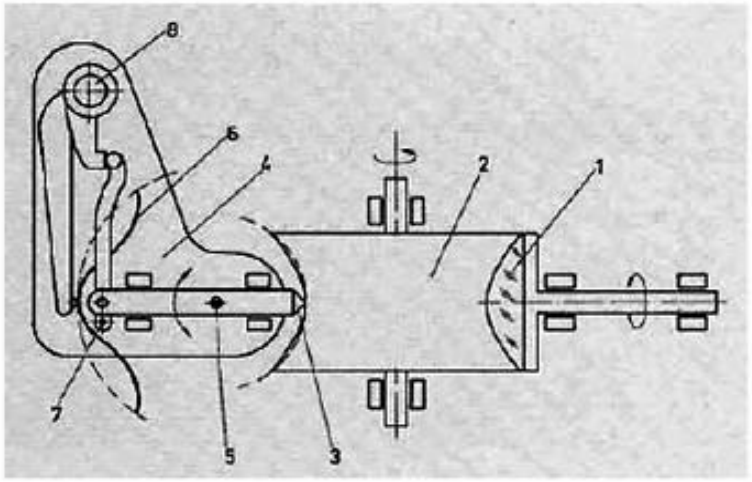

Figure 6: Principle of shape- copying machine as designed by Mackenson in the 1920s.[25]

The introduction of the computer around 1976 revolutionized optical fabrication. The technical possibility of continuous path control by computer initiated modern generating and polishing methods. With regard to generating, two approaches were chosen by the scientists and engineers at that time. The first approach was to keep most of the fundamental ideas from the time before computer era. One example of such machine is shown in the fig. 7. The aspherical element (2) below on a rotary table. The large vertical axis (9) is rotating around origin of the best fitting sphere. A position control system is moving the vertical axis forward and backward depending on the actual angle φ. This generates an additional shape correction $\Delta R = \Delta R(\varphi)$. As computers were rather limited in their performance in those days, only the control of ΔR was possible not that of R, but nevertheless it represented a huge evolutionary step toward better accuracy.

The second approach was to achieve the required accuracy with computing power and resolution of the numerically controlled drives. This approach became more and more the industrial standard, with increasing clock rate larger memories, and better resolutions of the gages.

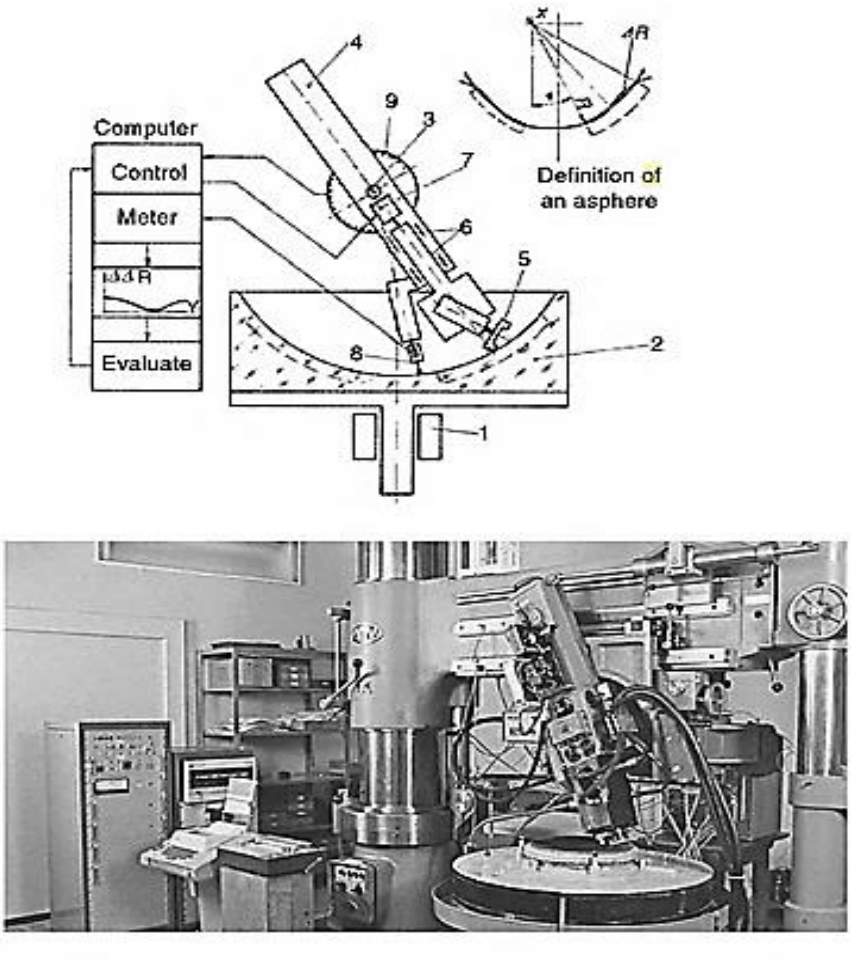

Figure 7: Principle and setup of the first computer grinding machines built by Zeiss [11]

2.7 Optical fabrication technologies

The ability to grind and polish steep aspheric surfaces to high quality is limited by the tools used for working the surface. The optician prefers to use large, stiff tools to get good natural smoothing, avoiding small scale surface errors. This is difficult for steep aspheres because the tools must have sufficient compliance to fit the aspheric surface, yet we wish the tools to be stiff so they wear down high regions on the surface.

The machining accuracy achievable, using different technologies over more than sixty years, is represented in fig. 8. This shows that each process expectation and perception continue to

improve with time. The same processes are continuously developed to be more efficient while achieving better surface quality output.

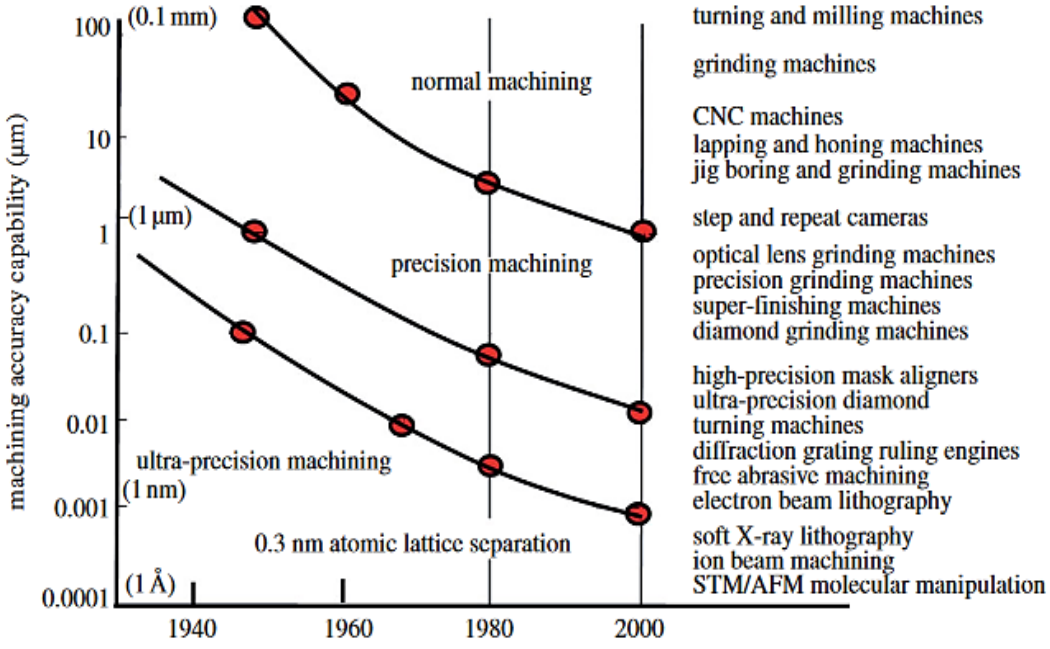

Figure 8: An interpretation of the Taniguchi curves, depicting the general improvement of machine accuracy capability with time during much of the twentieth century [12]

The different machining processes are single point diamond turning (SPDT), conventional fixed or loose abrasive grinding (FAG/LAG), computer numerical control polishing (CNC) and non-contact machining (Ion Beam Figuring - IBF). [14]

2.8 Material removal mechanisms

In general, material removal of brittle materials can be achieved through brittle, semi-ductile or ductile mode grinding. The material removal can be understood by analyzing the crack generation beneath a sharp intender, for example a single diamond. Small loads result in plastically deformed zone. Increasing the load creates radial and lateral cracks. If a lateral crack reaches the surface, a chip of material is removed (brittle mode). The remaining radial cracks determine the depth of subsurface damage. Working only in the regime of plastic or ductile removal mode requires highly stiff and accurately controlled machines. Plastic removal can be carried out by

fixed abrasive grinding or single- point diamond turning (SPDT), depending on the material properties.

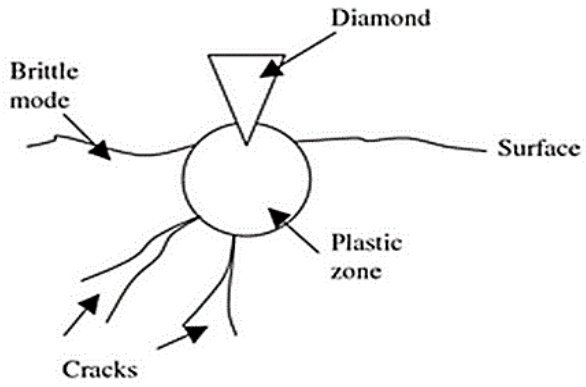

Figure 9: Principle of material removal within the plastic (ductile) and the brittle modes [18]

The most important parameter for the transition from brittle to ductile behavior in chip removal is the stress conditions in the workpiece material around the cutting edge. Ductile grinding mode has been reported to achieve minimal subsurface damage in brittle materials. For such materials, this "ductile" mode is limited in regards of removal rate as it is only achievable with very low critical depth of cut. For example, this depth of cut is 50 nm for Zerodur. [1]

2.9 Precision grinding process

Precision grinding ranks in between diamond turning and polishing in many respects. In this, a set of machine tool motions is controlled. Compared to diamond turning, the position of the cutting edge of the tool is less certain. At any time, one or more than one grains are in contact with a part. Grinding wheels tend to be compliant and can get worn off, which makes it more difficult to achieve the desired form accuracy compared with diamond turning. Besides these disadvantages, there are some notable advantages of precision grinding over diamond turning.

For small wheels and depths of cut, it can be used to work on brittle materials such as ceramics and glass in a ductile fashion (chip removal by ductile shearing of material, as in metal cutting). In some cases, the surface finish obtained with precision grinding is so good that polishing is unnecessary. The grinding process has the advantage over polishing of having higher removal rates and the ability to remove vastly different amounts of material from small areas. Thus, the grinding

operation is particularly suited to produce especially small complex shapes in materials that cannot be diamond turned.

2.9.1 Grinding modes for optical grinding

Different grinding modes have been described to machine aspherical surfaces. In fig. 10 we can see parallel grinding and cross grinding methods.

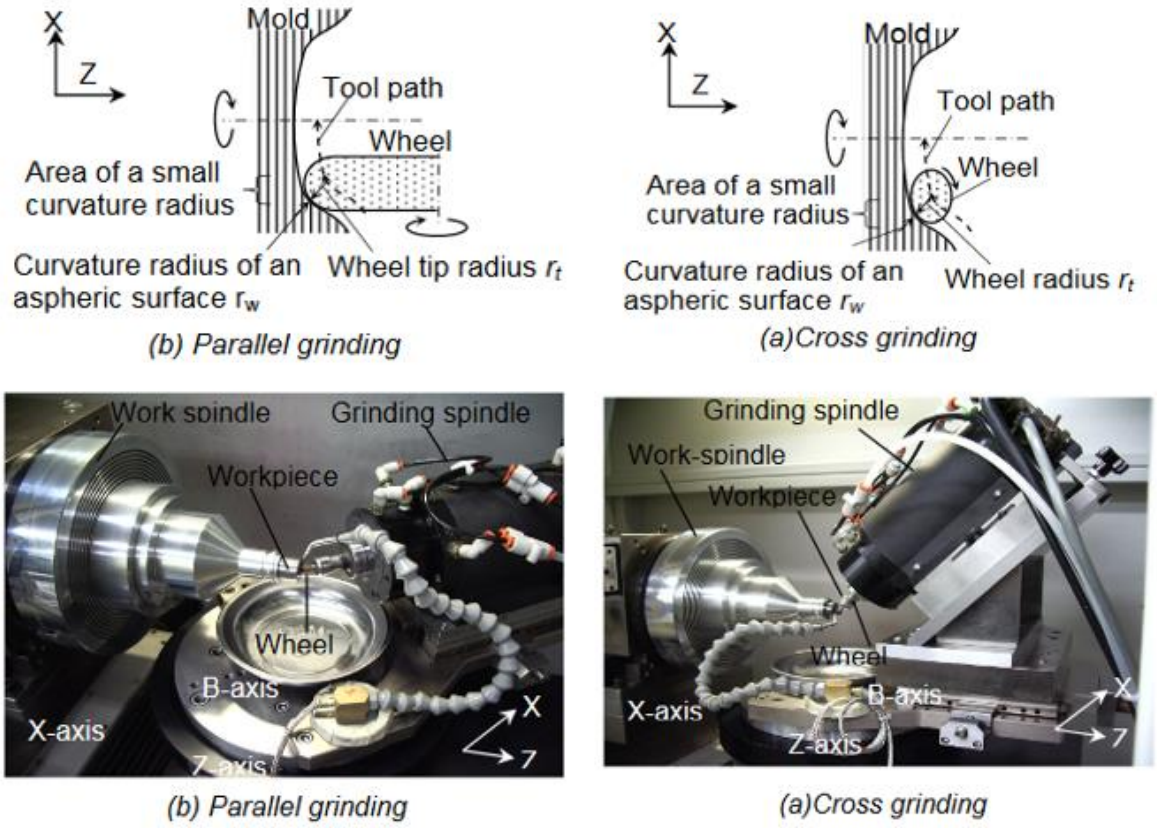

Figure 10: Different grinding modes for aspherical optics [23]

In parallel grinding method as its name suggests, the workpiece and grinding wheel revolution directions are parallel (a). In the cross grinding method (b), the grinding wheel revolution direction is perpendicular to the workpiece revolution direction. These grinding methods were compared on BK7 glass. The results show that ductile regimes enable higher removal rate in parallel grinding than in cross grinding. Different primary and secondary wheel wear zones were also identified. Variation of the grinding mode is achieved by tilting the grinding spindle at an angle with a spherical cup grinding wheel.

For aspherical optics, another grinding mode uses a cup grinding wheel. Figure 11 shows two ways of setting up the workpiece and the grinding wheel.

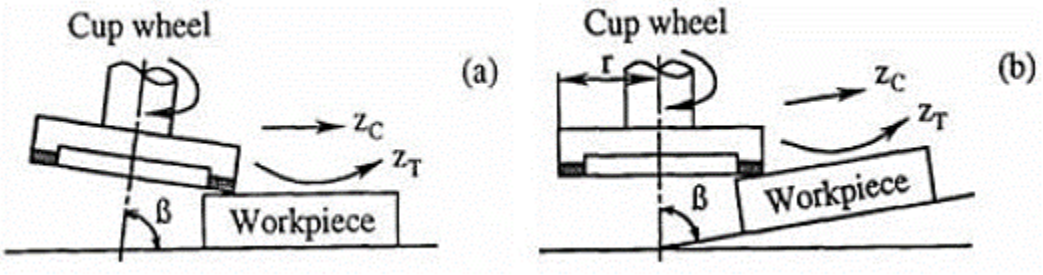

Figure 11: Different grinding modes for aspherical optics [21]

The cup wheel is fixed at a defined angle β in method (a). The workpiece is kept flat. The grinding wheel is controlled along the $z_c$direction. The depth is controlled along z_t to generate the required shape. In method (b), this time, it is the workpiece that is set at an angle. The grinding wheel is moved along z_c and z_t to generate the desired shape.

2.9.2 Grinding wheels

Grinding wheels are made of two materials, abrasive grains and a bonding material. They are produced by mixing the appropriate grain size of the abrasive with the required bonding material and pressed into shape. The abrasive grains do the actual cutting, and the bonding material holds the grains together and supports them while they cut. The cutting action of a grinding wheel is dependent on the bonding material, the abrasive type, grain size (grit size), wheel grade and the wheel structure. Selection of the right combination of these features is therefore essential for obtaining an optimum solution for different grinding tasks.

- Abrasives

Abrasive grains used for grinding wheels are very hard, highly refractory materials and are randomly oriented. Although brittle, these materials can withstand very high temperatures. They have the ability to fracture into smaller pieces when the cutting force increases. This phenomenon gives these abrasives a self-sharpening effect. During grinding, whenever dulling begins, abrasive fractures and new cutting points are created.

Four types of abrasives commonly used are aluminum-oxide or alumina (Al_2O_3), silicon carbide (SiC), cubic boron nitride (CBN), diamond, tungsten carbide (WC). Diamond wheels are suitable for machining non-ferrous metal.

- Bonding material

Beside the abrasive itself the bonding of abrasive tools is of major importance regarding the achievable quality and the overall grinding performance. The essential function of the bonding system is to hold the abrasive grains on the grinding tool as long as they are sharp, and to release them when they are blunt. The major bond systems are metal, plated, resin, vitrified and polyimide bonding.

The bond material is chosen to fit the material ground. For grinding optical components, a metal bonded grinding wheel needs a slow grinding process to avoid cracks due to the high pressure and hard bond. During grinding, whenever dulling begins, abrasive fractures and new cutting points are created.

The vitrified bond wheel loses its form quickly and is subject to damage under medium pressure. The resin bond wheel induces less damage to the grinding surface. It is made usually of phenolic resins with a dedicated structure depending on its applications. This grinding wheel type wears quite fast but it can be dressed and trued easily to keep its form. It cannot stand high temperatures. The polyimide bond wheel is similar to a resin bond wheel. However, a polyimide resin can be used with additives that improve the heat or wear resistance.

2.9.3 Nozzle and coolant selection

The choice of nozzle design and coolant type is important as it can influence grinding wheel wear and surface roughness. A laminar flow is obtained for Reynolds number below 2300. The Reynolds number, Re is calculated using equation 2 for a slot nozzle.

$$Re = \frac{\rho \times v_{slot} \times h_{slot}}{\eta} \quad (2)$$

Where η is the dynamic viscosity of the fluid (water = 0.001 Pa·s) and ρ is the density of the fluid (water = 1000 kg/m3). For a slot nozzle, the coolant velocity is v_{slot} and slot thickness is h_{slot}.

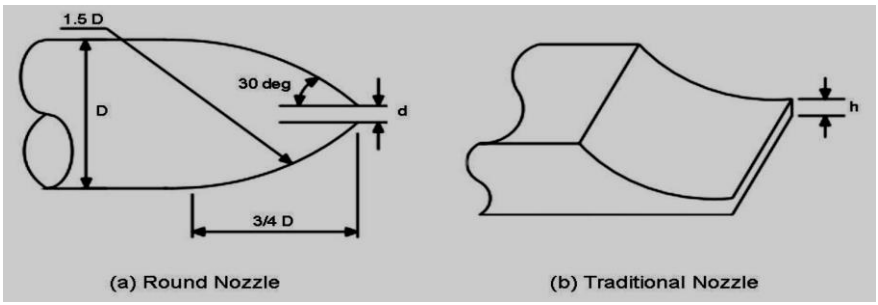

Figure 12- Different grinding nozzle designs [18]

The nozzle outlet height is called d and h for round and traditional nozzles respectively.

The round nozzle shape is proportional to its inlet diameter D. The use of a coherent flow helps to have a cooling efficiency that works at different distances to the grinding zone.

The grinding coolant reduces friction between the grinding wheel and the workpiece. It removes swarfs from the contact zone and reduces the risk of loading the grinding wheel.

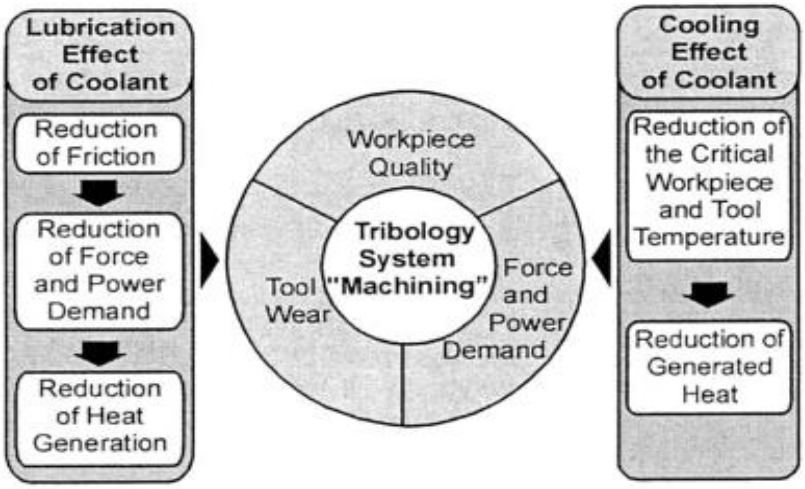

Figure 13: Tribology System 'Machining' [17]

The grinding contact zone and the grinding wheel need to be cooled down to avoid burn. Coolants are divided into oil based and water based. The water based emulsion coolant is a mix of water with low oil percentage. Water based emulsions are successfully used to grind ceramics. Additives are used to improve chemical and physical coolant characteristics. Other additives are anti-corrosion and anti-oxidants substances. Figure 13 summarizes the effects of coolant lubrication and cooling respectively; they are influenced by the type of coolant (oil, emulsion, solution) and its composition (emulsion concentration, additives)

2.9.4 Grinding process characterization

The grinding process parameters for a parallel grinding process are illustrated in fig. 14.

The material removal rate (Q_w) is calculated using equation 3:

$$Q_w = a_e \times f_r \times v_w \tag{3}$$

With a_e depth of cut, f_r feed per revolution or feed per step and v_w workpiece surface speed.

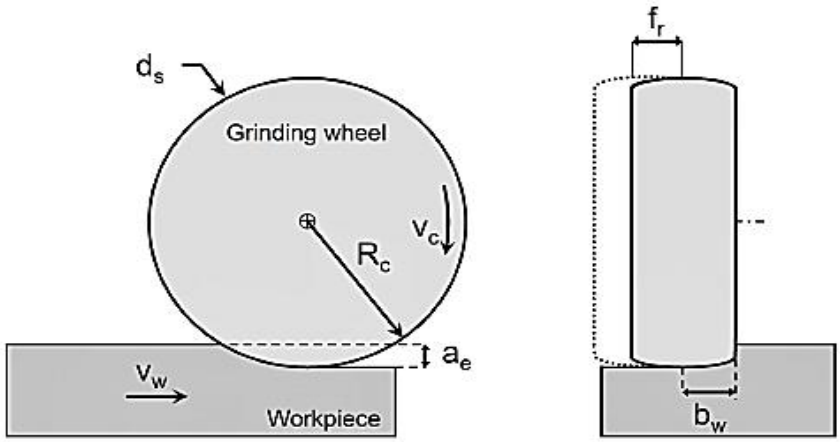

Figure 14: Grinding process parameters [9]

Grinding process is characterized by: contact length, number of active grits per unit area, maximum un-deformed chip thickness, equivalent chip thickness, grinding forces, grinding power, energy.

2.9.4.1 Grinding Energy

During grinding, the energy necessary to create a chip is transformed into different forms.

Figure 15 shows the three grinding process steps.

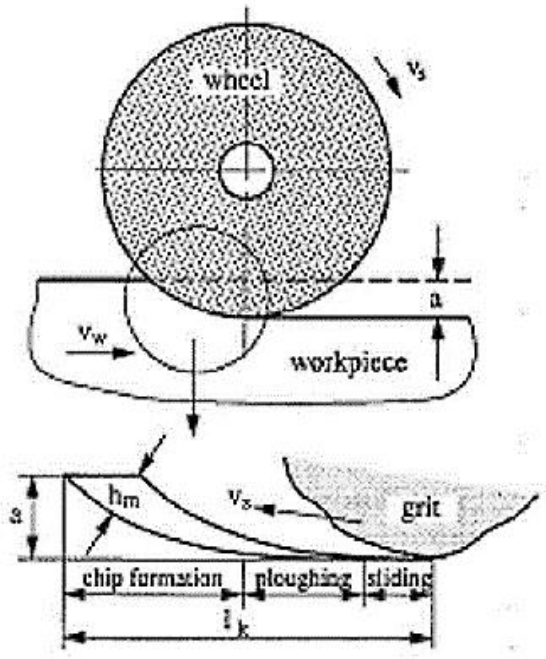

Figure 15: Grinding process steps [9]

The grinding process is separated into sliding, ploughing and chip formation. The grinding power has been divided in a similar way. When the grain depth of cut decreases, the sliding and ploughing powers proportions are more important. It leads to an increase in grinding energy. The main amount dissipates through thermal energy while a small amount generates residual stresses in the ground part. The specific grinding energy required to grind a material for particular machining conditions is calculated using equation 4:

$$e = \frac{F_t \times v_c}{Q_w} = \frac{P_c}{Q_w} \tag{4}$$

e −grinding energy, F_t −tnagential grinding force, Q_w −material removal rate, P_c −grinding power

2.10 Surface texture and form

A grinding mode is characterized using the surface roughness, peak to valley profile and surface patterns. The measurement of the surface roughness and surface profile are recommended by ISO (ISO 4288:1998, 1998).

2.11 Polishing

Smoothing the surface after the generating process is task of polishing. Polishing has to remove subsurface damage and to improve the surface roughness to the required level. For parts that are generated by ductile grinding or SPDT, the subsurface damage is nearly zero, and the amount to be remove is very small. Only smoothing of the surface is required. For parts generated by conventional grinding, like most optical elements, the subsurface damage layer determines the amount of the material that has to be removed by polishing.

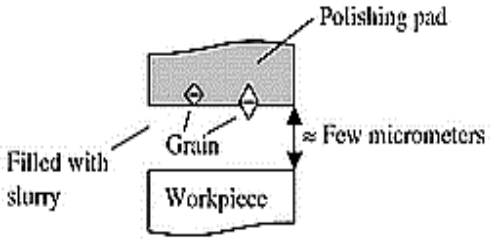

Figure 16: Schematic of the gap during polishing process

Polishing is an iterative “force controlled” process, in comparison with grinding and milling processes which are deterministic “position controlled” processes [5]. For a given combination of polishing tool, abrasive slurry and tool pressure, the amount of material removed increases with the amount of time spent over a given contact area. Preston equation (5) based on contact pressure, velocity and contact area, is used to predict material removal rates. For a specific polishing process, a Preston coefficient is calculated which varies with different type of material substrate. However, this approach is based on a consistent controlled polishing process.

$$\frac{dz}{dt} = c_p \cdot \frac{L}{A} \cdot \frac{ds}{dt} \tag{5}$$

Where, $\frac{dz}{dt}$ is the thickness change over time or removal rate $\left[\frac{m}{s}\right]$, $C_p$is the Pretson coefficient, L is the load (total normal force $[N]$), A is the surface area where the removal takes place $[m^2]$, and $\frac{ds}{dt}$ is the relative velocity of the workpiece to the tool $\left[\frac{m}{s}\right]$.

The principal challenge of polishing aspherics is the mis-match between tool and part, as the tool traverses the asphere's varying radius of curvature. This tends to drive the classical optician to very small tools for severe aspherics, resulting in surface defects and low removal-rates.

Currently optical process chains employ grinding for aspherisation, followed by sub-aperture CNC polishing, with the final form figure correction carried out with energy beam processes (fig. 17). Recent technological advances in grinding and final figure correction using Reactive Atom Plasma (RAP) technology have demonstrated significantly reduced processing times. These reductions have yet to be matched by advances in polishing technology; therefore currently, multiple high performance sub-aperture polishing machines are required, alongside a grinding and energy beam machine to achieve full utilization in optical manufacturing process chains.

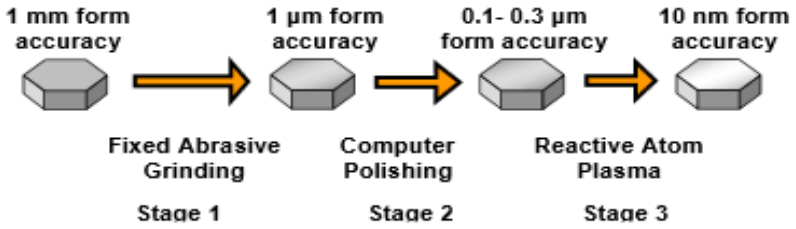

Figure 17: Current process chain for large optics [12]

Evans et al. [7] defined the four components for polishing processes as the tool, abrasive, carrier fluid and workpiece. The tool or polishing pad is generally made of pitch, polyurethane or cloth.

2.12 Local correction

Due to the non-perfect polishing step or based on the required final surface specifications the aspheric element has to pass a third process step, local correction. Residual surface deviations from the nominal shape have to be removed by this process step. As shown in the figure 18 a small sub-aperture tool is moving across the surface in a meander or spiral path. The tool itself is characterized by a tool function, which is the removal rate at a fixed position. The desired removal $R(x)$ is the difference between the nominal and real shapes.

For the local correction, the tool described by function c(x) has to be moved in a computer-controlled fashion across the surface, such that the desired mass removal $R(x)$ will be achieved.

One parameter to optimize the tool path is the dwell time. The equation for the local correction can be written as:

$$R(x) = \int c(x - x')s(x')dx',$$

$R(x)$ −desired removal rate (e.g. surface from intereferometry) , $c(x - x')$ −tool function(to be measured) , $s(x)$ −to be determined. To get a stable convergence of the local correction process, the following equation have to be fulfilled:

- Stability of the process, tool wear and slurry(if applied);
- Tool function(process, symmetry);
- Accuracy and stability of the machine;
- Performance of algorithm; and
- Accuracy of the related metrology

The goal is to mention all the parameters above. This holds for all the methods involved like: CCP, MRF, fluid jet, or IBF.

Local computer- controlled polishing (CCP) was developed in particular to polish conical aspheres for astronomy. The CCP method is applied in customized setups by several optical companies and is also commercially available from Zeeko/ Staisloh.

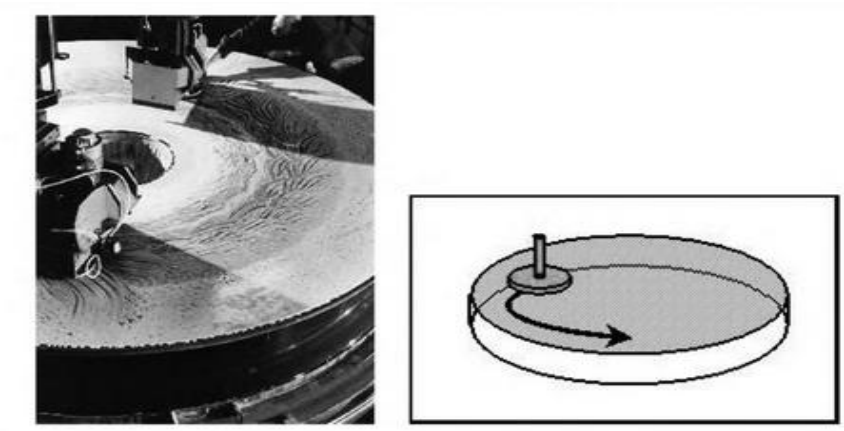

Figure 18: Left- CCP process of the NTT ESO 3.5m mirror; right, principle of the CCP [14]

Fluid Jet Polishing (FJP), which Compared to CCP there is no wear of the tool itself and a nearly constant removal rate by working over the rim of the part, Magnetorheological finishing

(MRF), compared to CCP, there is no wear of tool itself (like FJP), perfect adaptation of the liquid to the workpiece shape, and a nearly constant removal rate by working over the rim of the part (only small surface deviation at the rim), Ion beam Figuring (IBF) Compared to CCP there is no wear of the tool itself (like FJP, MRF), a perfect adaptation to the workpiece shape, a nearly constant removal rate by working over the rim of the part, and no print through (quilting) for lightweight structures.

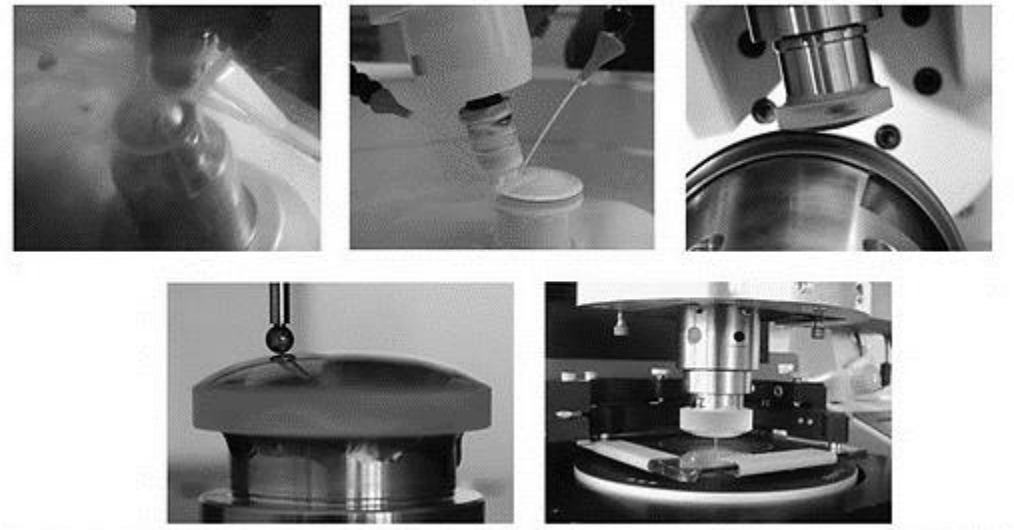

Figure 19: Example of a process chain for processing aspheres including related metrology [14]

In table 1 is given an overview specifications and characteristics of the different processes (typical values in production), courtesy of SCHOTT.

Process	Batch size	Dia. $[mm]$	Shape devi. $[nm]$PV	Surface rough. $[nm]rms$	Adv.	Disadv.	Main cost driver
Grinding	$< 10^4$	2-400	1000	50-1000	fast generation process	SSD	Size, accuracy
Diamond turning	$< 10^3$	2-400	100	5-20	no SSD, for IR sufficient roughness	Subsurface roughness	size
Speed/ pitch polishing	$< 10^4$	10-300	300	0.2-0.5	very low subsurface roughness	correction of local surface deviations	size
CCP	$< 10^3$	5-8000	30	0.5	30 years of experience	tool wear, edge roll off	size
MRF	$< 10^3$	5-500	10	0.3	no edge roll, no tool wear	centre artefacts for $r - \varphi$ tool path	size, fluid
FJP	$< 10^3$	5-240	30	0.5	No edge roll off	stability of tool print	size
IBF	$< 10^3$	-	5	0.2	No edge roll off	low removal rate	vacuum

Table 1: Overview specifications and characteristics of the different processes (typical values in production)

Chapter 3: Overview of material properties and material models

This overview indicates how relevant material properties are for optical system performance. The most often used optical material classes are glasses, crystals, polycrystalline ceramics, and polymers. The development of materials for aspheres is driven by costs issues, by the production technology used, such as precision molding, diamond turning and computerized numerical control (CNC) machining.

Although costs are the driver, materials for aspheres are still specified by their main properties according to their application and production or processing requirements. The most important physical properties of any optical material are the refractive index n_d, the Abbe number ν_d,and different partial dispersion values P. Note that the Abbe number:

$$v_d = \frac{n_d - 1}{D} \tag{6}$$

where D is the dispersion term $D = n_f - n_c$. Thus small Abbe numbers describe high-dispersive material. Other important material parameters to be considered are the transmission values and the scattering characteristics in the ultraviolet (UV), visual (VIS) and infrared part of the spectrum. Stress optical coefficient K and birefringence are of secondary relevance but clearly must be considered by the designer.

Chemical resistance of materials against water, acids and bases are of relevance, not only for a specific application, but also with respect to processing steps like grinding, polishing and cleaning.

Mechanical properties, such as hardness (Knoop HK) and Young's modulus (E) are important for grinding and polishing, but they also determine the scratch and stress resistance of optical devices.

With the use of Young's modulus E, the Poission ratio μ, and density ρ, we can obtain the following terms:

- Specific thermal stress for the maximal expected stress in glass for a special local temperature difference of 1K:

$$\varphi_w = \frac{\alpha \cdot E}{1 - \mu} \tag{7}$$

- The specific heat conductivity

$$\kappa = \frac{\lambda}{c_p \cdot \rho} \tag{8}$$

describes heat diffusion in materials. The actual heat flow also depends (besides κ) on the mechanical boundary conditions, for example whether the lens mount is kept at a constant temperature or, in contrast, is actively heated. It allows calculation of the temperature gradient inside lenses as a function of time. Consequently the local refractive index of glass varies with time, which could have a serious impact on the imaging properties of a lens system.

To date the use of glass ceramics has been restricted to reflective components. However, the use of mirror systems, particularly in combination with aspherical surfaces, is growing tremendously in many application fields, where optical systems with a large aperture, but a small field of view and polychromatic illumination, are required. Besides astronomy, which is traditional domain of reflective systems, instruments for space, lithography, and military applications are prominent examples.

Polymer-nano-composites and fluids are offering features and may attract more attention in the future, but they are not really in use today due to their lack of maturity as a technology. However, fluids in particular could play a role in adaptive optics of the next generation.

The different material types can be classified primarily by refractive index and Abbe number, which describes the dispersion. In fig. 20 typical areas of the different material classes are shown.

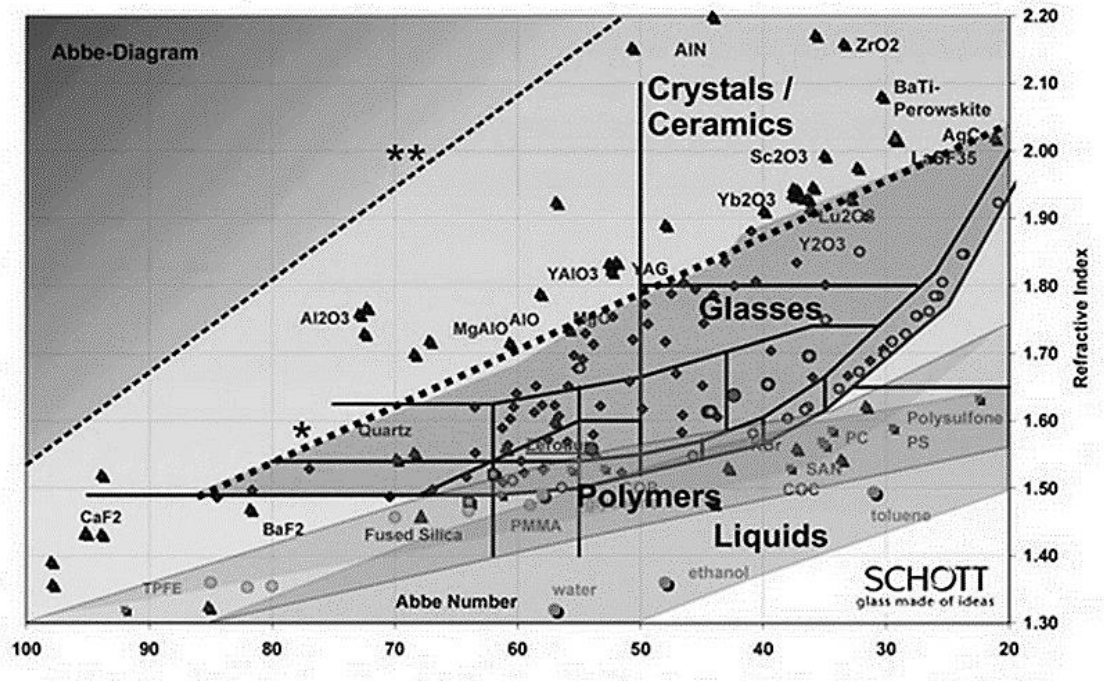

Figure 20: Abbe diagram of optical materials (fluids, polymers, glasses, crystals)

Fluids and polymers are located mainly in the lower right field of high dispersion and low refractive index values. Glasses are typically above this field, and only crystalline materials have the potential to exceed the glass field limit to higher refractive indices. The two lines, the so called magic lines indicate borderlines. Beyond these lines, normal glasses (* dotted line) or crystals (** hatched line) are not stable or do not exist at all.

3.1 Mirror substrate materials

The main optical materials, that have been considered, for making large telescope segments are: Glass (ULE), Glass ceramic (ZERODUR, Clearceram), Ceramics (SiC, CVD SiC) and some others materials such as Beryllium. For example, Keck and GTC telescopes have been made out of zero expansion glass ceramics. Silicon carbide is also a potential material.[9] It is stiffer than ZERODUR. The support structure, therefore the whole telescope, can be made lighter. The raw material cost and its dimensional stability compared to glass-ceramics through time are major concerns.

The comparison of the potential materials can be done by using different ratios of mechanical and thermal properties. These ratios highlight the behavior of each material to machining. For

example, the specific stiffness $\left(\rho/_E\right)$ relates to the flexion of the component under high pressure. The steady state thermal distortion $\left(\alpha/_k\right)$ corresponds to the thermal expansion under high grinding temperature.

	density *r* [kg m^{-3}]	Elastic modulus *E* [GPa]	Thermal conductivity *k* [W m^{-1} K^{-1}]	*CTE* [x10^{-6} K^{-1}]
SiSiC	2890	391.0	160.00	2.40
SSiC	3200	450.0	120.00	2.00
CVD SiC	3200	466.0	290.00	2.20
Zerodur	2530	91.0	1.64	0.05
ULE	2200	67.0	1.30	0.03
BK7	2530	80.7	1.12	7.10
NSF-15	2920	90.0	1.05	7.50
Quartz	2200	70.0	1.40	0.50
Fused silica	2200	72.0	1.31	0.50
Polysilicon	2300	110.0	150.00	3.80
Silicon	2330	131.0	163.30	2.60
Beryllium	1850	287.0	190.00	11.30
Aluminium	2700	68.0	170.00	23.60
Invar 36	8000	146.0	10.20	1.30

Table 2: Material properties of selected materials for optical applications

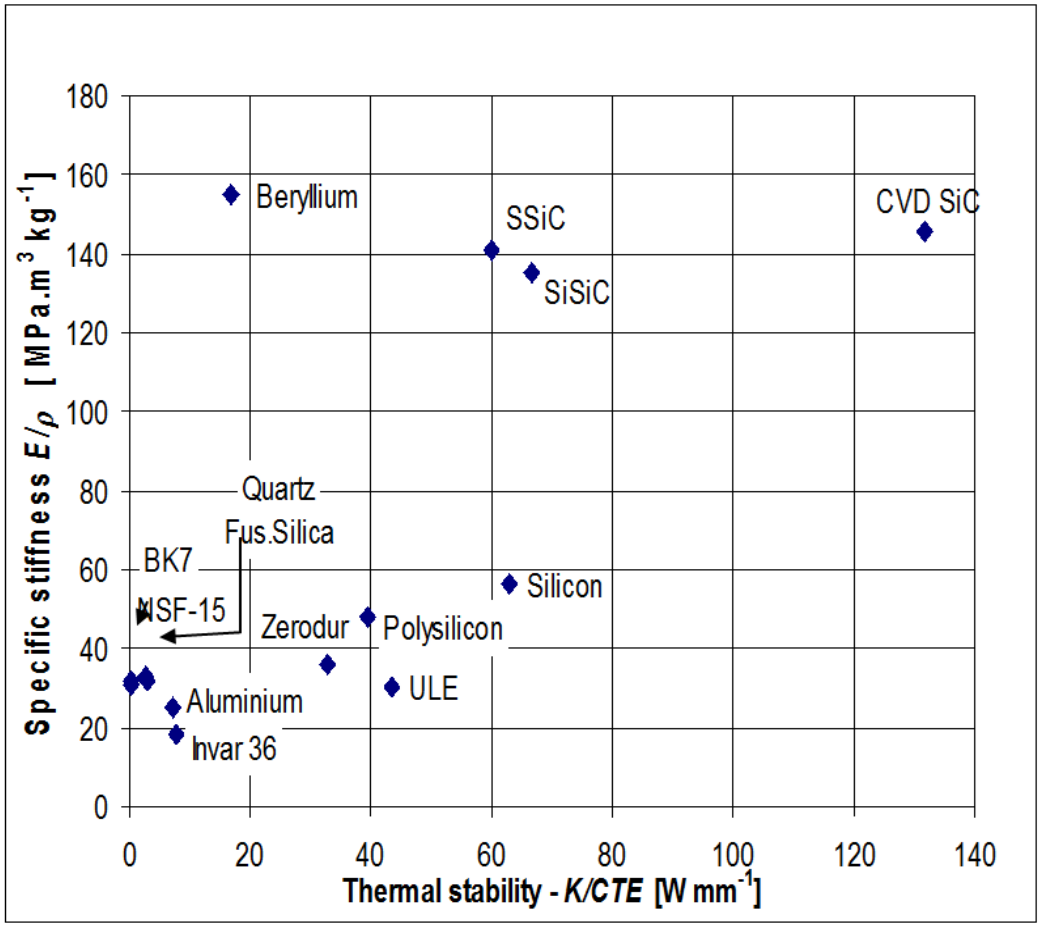

Figure 21: Material properties of selected materials for optical applications

The application of materials based on silicon carbide should be a solution to many of the shortcomings that arise from the use of conventional materials. Silicon carbide (SiC) has excellent mechanical and thermal properties when compared to other materials. Its most important material properties include low density, high modulus, a low coefficient of thermal expansion and high thermal conductivity. Depending on the specific application, a high value of fracture stiffness and resistance to stress corrosion may also be relevant. These features lead to slow crack growth and long-term reliability under static and dynamic loading. Unfortunately, the properties that make SiC attractive in terms of design prevent its wider use in applications where low-cost and relatively short delivery times are required. A comparison of selected materials is presented in table 2 and figure 21.

3.1.1 Glass ceramics

SCHOTT invented ZERODUR, the zero expansion glass ceramic, in 1968 and thus introduced a new era for various applications, of which the most challenging ones are telescope mirror substrates for astronomy. ZERODUR is an inorganic, non-porous glass ceramic, characterized by a phase of evenly distributed nano-crystals within a residual glass phase. ZERODUR contains about 70-78 weight percent crystalline phase with a high quartz structure. This crystalline phase has a negative linear thermal expansion, while that of the glass phase is positive. The crystals have an average size of about 50 nm.

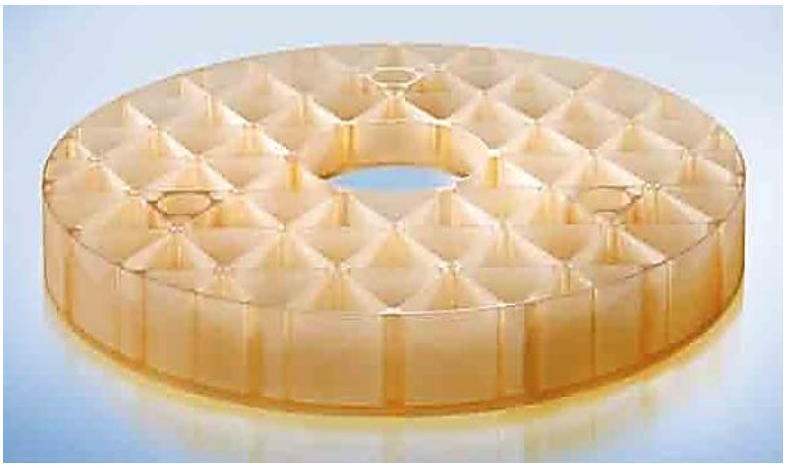

Figure 22: ZERODUR [19]

The key properties of Zerodur are:

- Extremely low coefficient of thermal expansion (CTE) for a wide temperature range
- Excellent CTE homogeneity throughout the total volume
- Very low content of imperfections
- Wide range of precise geometrical shapes
- Extremely smooth surface with residual roughness below 1 nm
- Excellent chemical stability

All these properties are realized for small components as well as for astronomy telescope mirror blanks weighting several tons with extraordinary reproducibility. Zerodur is supplied in the form of disks, rectangular blocks, prisms, rods and any other customer-specific cut piece geometry. The CNC grinding machines allow for precise fabrication of parts of up to 4.5 m in diameter.

Diamond tools are used for machining Zerodur. Standard tool diamond grain sizes are between D64 and D251. Zerodur withstands loads of up to 10 MPa without any difficulty, as long as its surfaces is not severely damaged. For higher loads, is recommend analysis on the basis of the Weibull model and introducing precautions to prevent degrading of surface quality. Even higher loads than approximately 50 MPa may require special surface treatments, like optical polishing or acid etching (fig. 23)

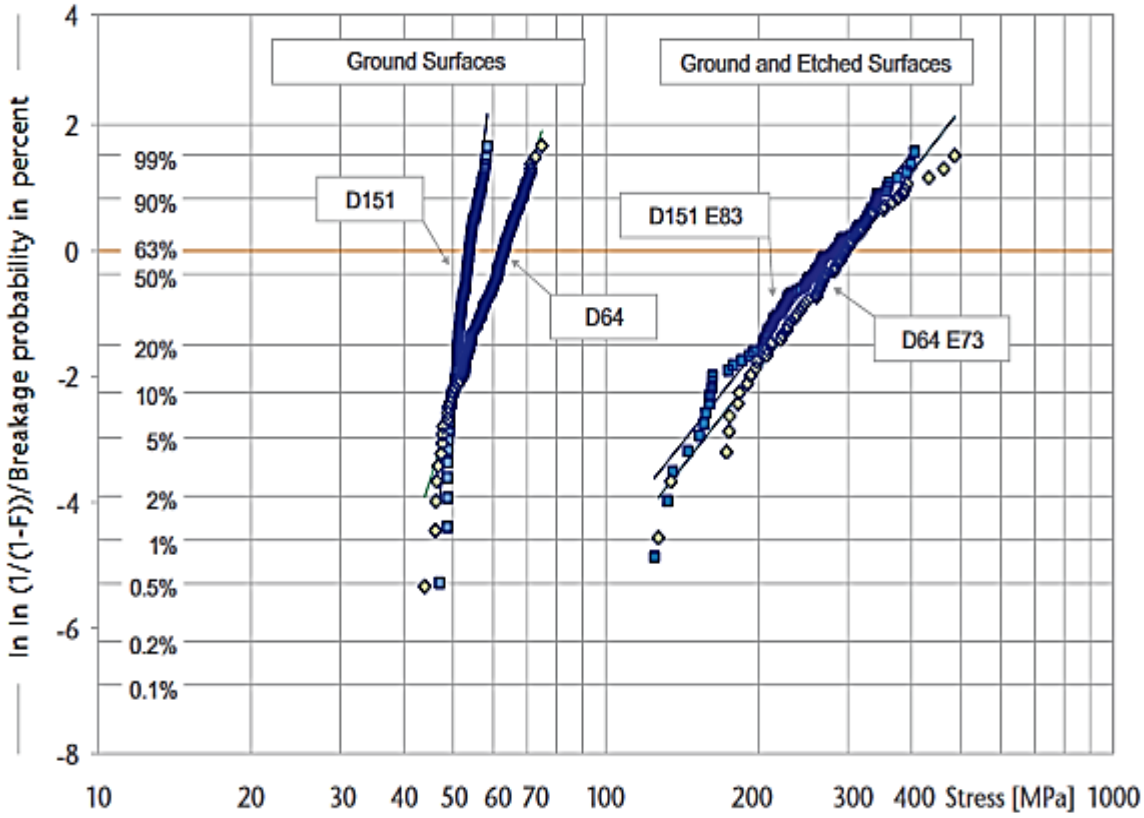

Figure 23: ZERODUR cumulative breakage probability distributions D64 and D151 are diamond grain size distributions; E83 denominates the layer thickness in $\boldsymbol{\mu m}$ etched off - here 83 $\boldsymbol{\mu m}$ [19]

In this table are shown some of material properties of Zerodur.

Properties	ZERODUR
Density $[kg/m^3]$	2.53×10^{-9}
Young's Modulus E$[MPa]$	90300
Poisson's Ratio μ	0.24
Coefficient of thermal expansion α $[1/K]$	0
Heat Capacity $C_p(20℃)[J/kg \times K]$	8×10^{-4}
Thermal Conductivity $\lambda_{90℃}[W/m \cdot K]$	1.46
Maximum Application Temperature $[K]$	873.15

Table 3: Properties of ZERODUR

3.2 Materials used for blocking the optic

Most optical fabrication processes begin with the extremely important consideration of holding onto the part during subsequent fabrication steps. Numerous factors must be considered when choosing the support method: part size, thickness, shape, expansion coefficient, and the direction and magnitude of applied forces. The support should not stress the optic, otherwise when the part is finished and unmounted (or "de-blocked"), it will distort by "springing" into its stress-free condition. However, the part must be held rigidly enough to resist the forces of the various surfacing methods.

The lateral forces can be large, so the part must be held quite firmly to a rigid plate or fixture. This plate, called the blocking body, or "block", can be made of various materials depending on the process. It is usually made of aluminum, steel, cast iron, or glass, brass with rigidity being the most important factor. The two principal methods for holding the part to the block are to use adhesives or mechanical attachments at the edge.

The ideal adhesive would provide a rigid bond with little stress, and it should allow the part to be easily removable. Most adhesives cannot achieve all three requirements well, so optician must choose, depending on which consideration is most critical. For the generation processes using high-speed diamond tools, rigidity and ease of removal are usually the dominant criteria with

higher stress being allowed. The effects of this stress are then removed in the subsequent processes of grinding and polishing, where a less stressful blocking method is employed.

3.2.1 Waxes, Pitch, and Cements

Blocking of "plano" and spherical parts up to around 100 mm in diameter is done with a variety of waxes, both natural and synthetic. These are heated to a liquid before applying to the block, or heated by the block itself. The glass parts are then warmed and placed on the waxed block. For heat sensitive materials, wax can be dissolved in solvent before applying to the block. The great advantage of waxes is that they hold the glass quite firmly and are also easily removable by dissolving them in common solvents. Most waxes, however, impart large stresses due to their shrinkage. This requires parts to be de-blocked after generating, and subsequently re-blocked with a less stressful substance for grinding and polishing.

The most generally used soft wax is made from beeswax and turpentine mixed in the ratio of about 5 to 1; this is sometimes colored red, from which wax takes its name.

Pitch remains the blocking material of choice when the parts cannot be highly stressed. Pitch is an outstanding material, and is used in the optics shop both for blocking and for facing polishing tools.

Cements such as epoxies and RTV's bond very well, but are extremely difficult to de-block and remove. There are also some UV curable cements that can provide low stress blocking and can be removed with hot water.

Chapter 4: Manufacturing process

The traditional steps for making an aspheric surface are to first generate and grind to a spherical surface by using the same methods as for spherical surfaces as follow:

- Rough shaping: The initial blank is manufactured, typically to within a few millimeters of final dimensions.
- Support: The optics must be held for the subsequent operations. Much of the difficulty in fabrication comes from the requirements of the support.
- Generating: The blank is machined, typically with diamond tools, to within 1-0.1 mm of finished dimensions.

And then then the surface is "aspherized" by grinding or polishing with a specially designed tool, stroke, or machine (see chapter 2.7- 2.13 for more details).

There are a variety of methods for aspherizing. Full size compliant tools can be used with the contact area defined as petals that give the desired removal as the part is rotated underneath. Full size metal tools with the inverse aspheric curve are used for "plunge grinding" of small parts. Most commonly, smaller laps are used, and the dwell is adjusted based on the aspheric curve to be ground in. The aspherizing process is usually monitored with mechanical measurements, such as spherometry or profilometry.

- Grinding

Most aspheric surfaces are produced by highly skilled opticians using small tools and conventional machinery. In TOPTEC for our experiments we used CNC sub-aperture grinding, which machining process gives a surface roughness better than 3Å.

- Computer Controlled Polishing- CCP

There are a number of methods being developed that integrate computer technology with radically different polishing methods that can rapidly produce aspheric surfaces. The first of these is the computer controlled polishing (CCP) method. This is essentially a traditional small tool method where the tool is driven in an orbital motion producing, on average, a known wear profile. This wear profile is applied to the measured errors in a surface to produce a tool path that essentially rubs longer on the high areas and less on the low areas, but in a precise relative way that can rapidly improve the figure. Sophisticated, proprietary computer algorithms are used to determine the

optimal machine motions from the surface measurement and removal function (see chapter 2.12 for more details).

For our experiments we used CCP with sub-aperture polyurethane pad.

Chapter 5: Design of experiments

Centre TOPTEC is responsible for realization of two main mirrors (M1 and M2) of METIS telescope for ESA. Both the primary M1 mirror and secondary M2 mirror are designed as concave aspherical surfaces with an approximately 40 micrometers departure from the best fit sphere with an outer diameter of 218 mm and inner diameter of 128 mm for M2. Mirror M1 has 125 mm outer diameter and 88 mm inner diameter. In the fig. 24 are presented dimensions of mirror M2 with which we are going to perform experiments and FEM model as well.

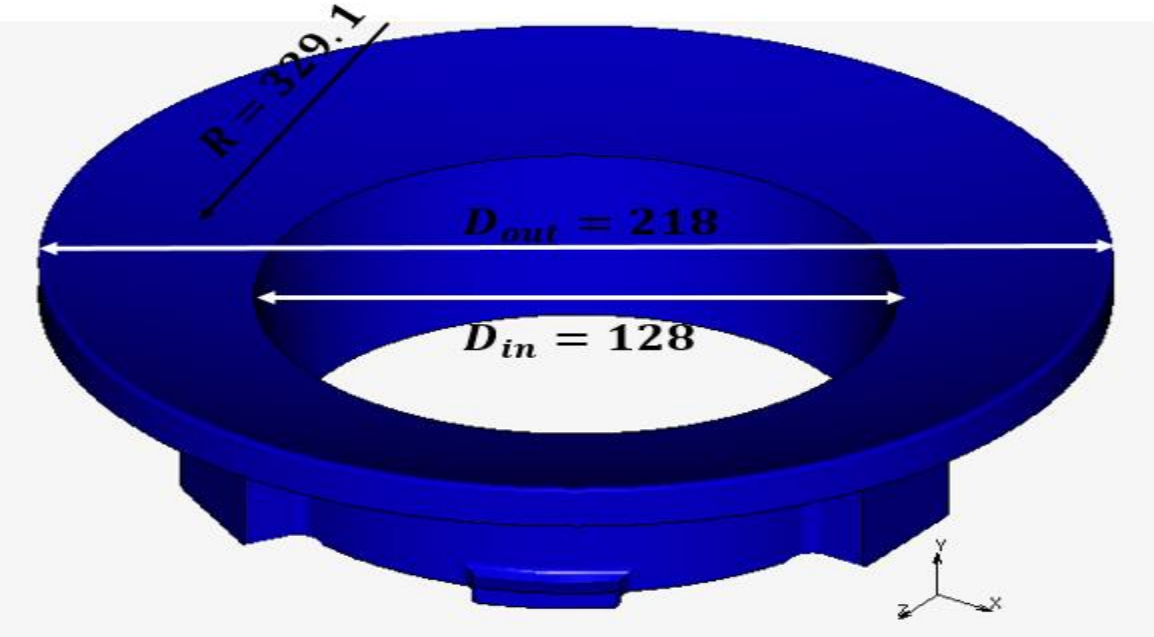

Figure 24: Dimensions of the mirror M2

Both mirrors surface shape is a mild asphere with departure of approx. 40 mm from the best fit sphere, therefore it is necessary to apply sub-aperture grinding and polishing techniques that TOPTEC is equipped with. Most challenging within this project is to reach the optical qualities of the mirrors that stands in their surface form (120 nm PV) and micro-roughness (0.3 nm) together with their total weight that is demanded as < 1kg for both mirrors in total. For this purposes TOPTEC is equipped with state-of-the-art stitching interferometer (enabling of aspheric surface form characterization) and white light interferometer (measurement of micro-roughness with 0.1 nm resolution).

The aspherical mirror was made of Zerodur supplied by SCHOTT. The holder was made either by brass or aluminum, and for gluing of the mirror to the holder we used red wax. The Zerodur disk (aluminum disk) of diameter 160mm and thickness 14.8mm is cemented on the holder by Loctile 9455, which in our simulations is neglected. In fig. 25 are shown dimensions for brass holder and Zerodur disk, which are same for aluminum holder and disk as well.

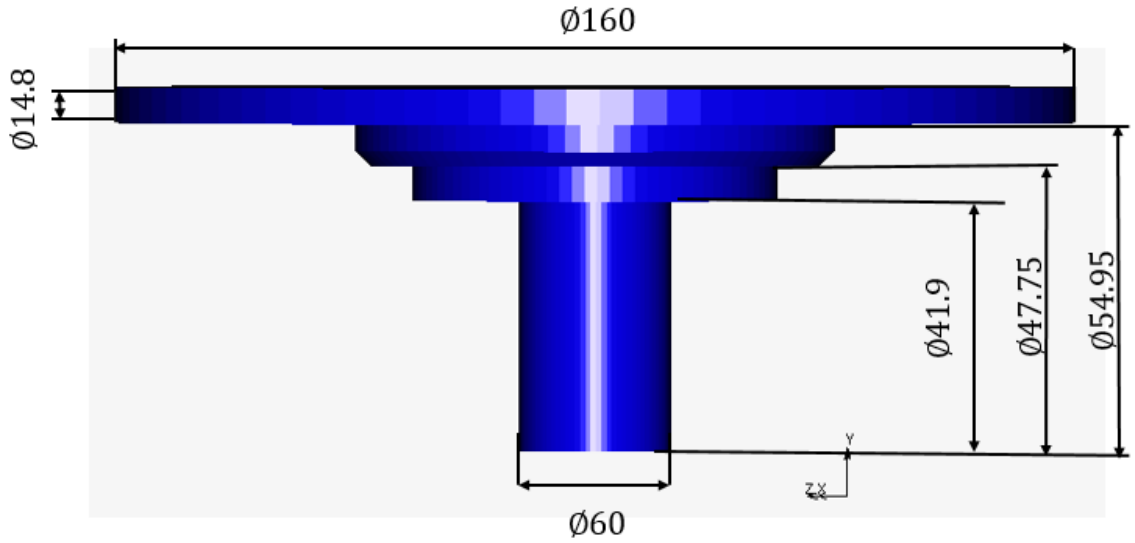

Figure 25: Dimensions of CNC holder and Zerodur disk

In the fig. 26 is shown the mirror bonded to the holder while measuring surface shape in LuphoScan.

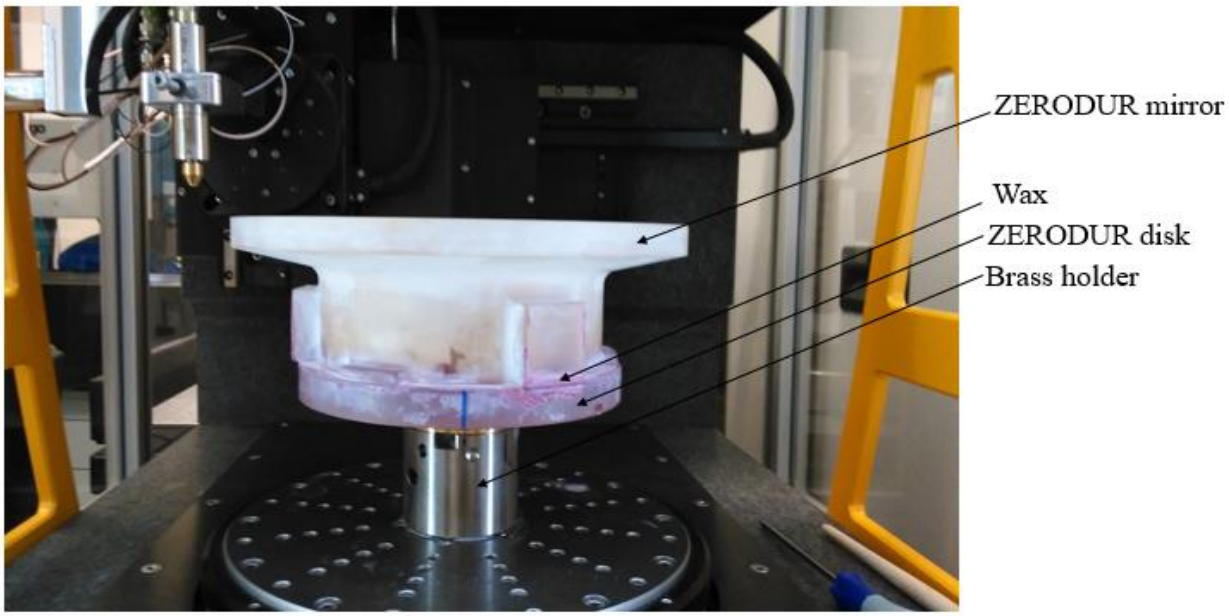

Figure 26: ZERODUR mirror on ZERODUR disk and brass holder placed in LuphoScan

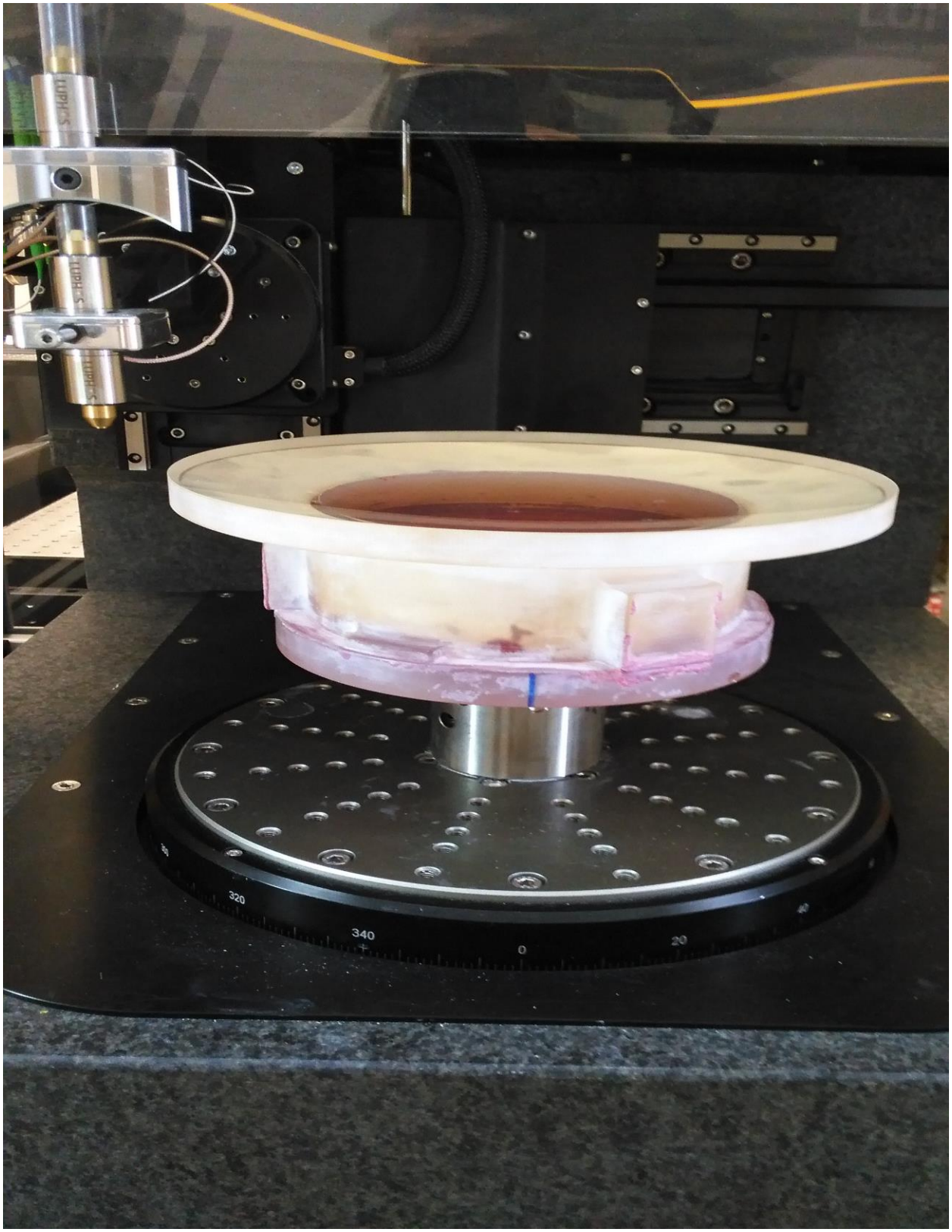

Figure 27: Top view of the mirror on holder placed in LuphoScan.

Firstly, experiments were done using aluminum holder and disk. But after finishing of manufacturing process and removing the mirror from the holder there was a deformation of the mirror. For this case we preformed FEM and when compared the results from both experiments and FEM the same behavior was observed. So, we had to realize where the problem is, and in doing so we it was proposed to make a change in the disk, where instead of aluminum disk to be used a Zerodur disk.

After doing FEM for the case of Zerodur disk we got better results and this was proved also with the experiments, which we are going to describe in details.

By consecutive steps of bonding of the Zerodur mirror to the holder we want to show how much this process is going influence the quality of the final shape of the mirror.

Firstly, we heat up the wax to its melting point, 70℃ respectively, process which takes 100 sec. The Zerodur mirror that has to be glued is grounded and polished at the side of contact with wax. So, after placing the mirror to the melted wax we wait for 600 sec and then we start cooling of the wax and holder for 3300 sec. Now we can say that the mirror is strictly bond to the holder but because of the relaxation time of the red wax which we assumed to be 3400 sec we have to let the bonded mirror to stay for 4 days and then perform the consecutive steps of manufacturing process of the mirror, i.e. grinding and polishing. When this is reached we put the holder with the mirror in the Precise Machine to undergo the subsequent process of CNC grinding.

During the manufacturing (grinding and polishing) we fill the gap of ring mirror by cementing additional Zerodur glass. We do so to prevent any damage of the edges, since they are exposed to sub-aperture movement and on the edges it is so easy to be caused the unwanted damage. This gap on the fig. 27 is colored in light red.

Chapter 6: Numerical simulations of the manufacturing process

This chapter discusses the numerical simulations of consecutive steps of bonding of the mirror to the holder. The numerical simulation of our process are performed in MSC Marc.

MSC Marc is a non-linear finite element analysis (FEA) program that enables to assess the structural integrity and performance of parts undergoing large permanent deformations as a result of thermal or structural load. The types of deformations the program can study include geometric nonlinearities (metals bending) and material nonlinearities (elastomers and metals that yield under structural or thermal loading)

The nonlinearities may be due to either material behavior, large deformation, or boundary conditions. Physical problems in one, two, or three dimensions can be modeled using a variety of elements. These elements include trusses, beams, shells, and solids.

So, we chose this tool believing that it carries out the best analyses for our problem since we are dealing with non- linear problem, sources of which comes from the geometry, material (viscoelastic), and contact bodies.

6.1.1 Meshing

Mesh definition is the process of converting a physical problem into discrete geometric entities for the purpose of analysis. Before a body can undergo finite element analysis, it must be modeled into discrete physical elements. For MSC Marc to have a valid mesh definition, the nodes must have geometric coordinates and must be connected to an element.

To perform meshing for our geometry we used the quadrilateral elements. The mesh consists of 102146 nodes and 87114 quadrilateral elements (fig. 28).

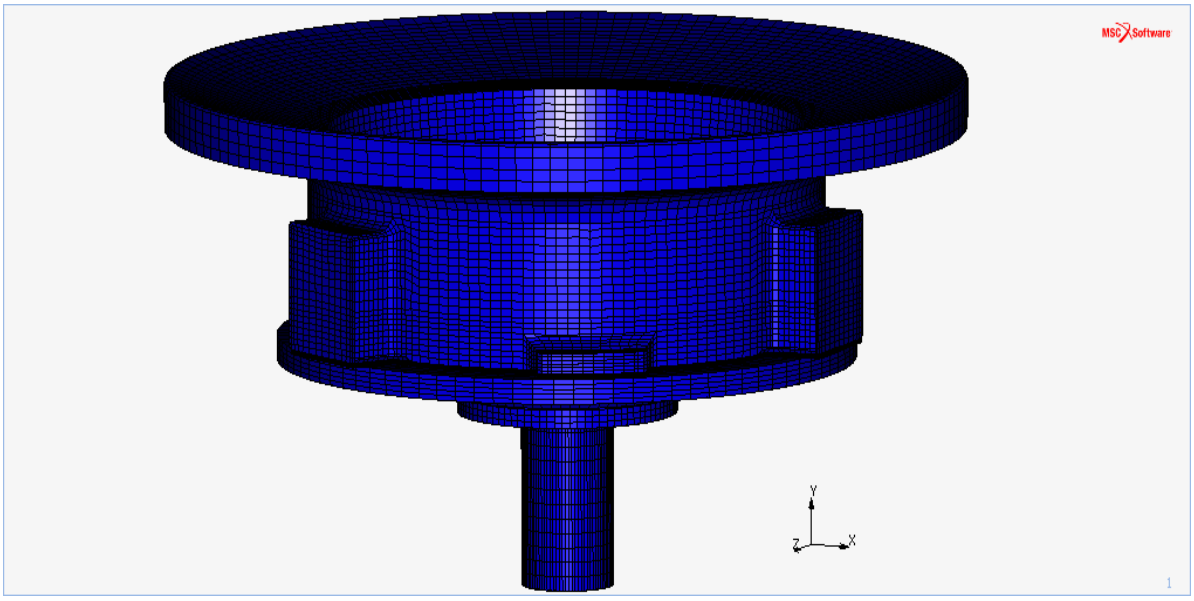

Figure 28: 3D mesh of the mirror and holder

Another important feature in MSC Marc is Local Adaptivity. The adaptive mesh generation capability increases the number of elements and nodes to improve the accuracy of the solution. The capability is applicable for both linear elastic analysis and for nonlinear analysis. In the figure 29 it is shown local adaptive mesh on the center of the holder.

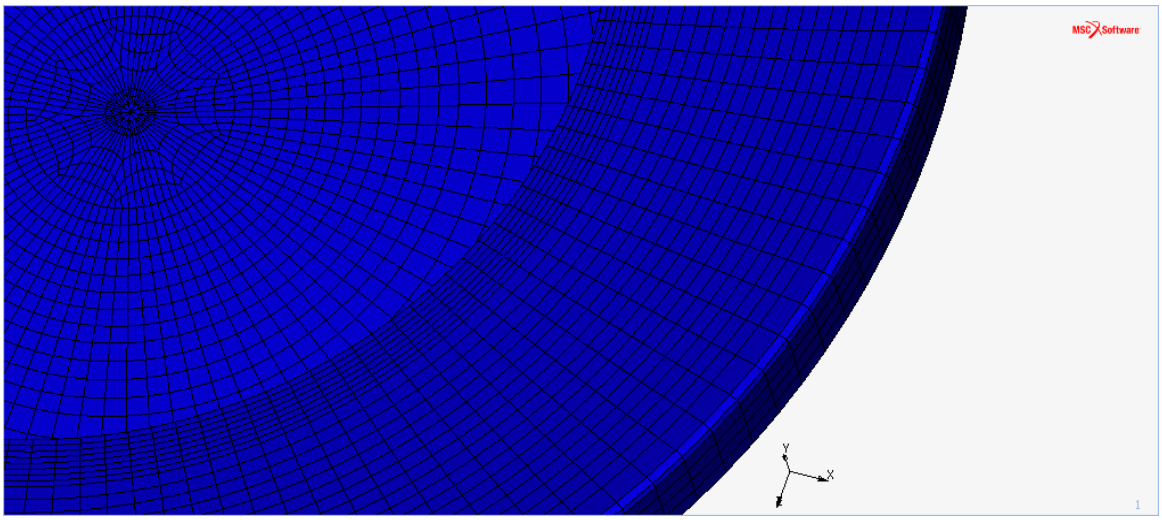

Figure 29: Closer view of adaptive mesh (Centre of the Geometry)

6.1.2 Material Properties

Marc is capable of handling problems with either isotropic linear elastic material behavior or anisotropic linear elastic material behavior. Most linear elastic materials are assumed to be isotropic (their elastic properties are the same in all directions). To characterize the behavior of an isotropic linear elastic material at constant temperatures, we need only to specify Young's modulus and Poisson's ratio. It can be shown that for an isotropic material the shear modulus G can be easily calculated if the modulus of elasticity E and Poisson's ratio ν are known by using the relationship:

$$G = \frac{E}{[2 \times (1 + \nu)]} \tag{9}$$

The input material properties for ZERODUR are listed in table 3, while for brass are listed in the table 4, and in table 5 of aluminum.

Properties	**Brass**
Mass Density ρ $[kg/m^3]$	8525
Young's Modulus E $[MPa]$	97000
Poisson's Ratio μ	0.31
Thermal Expansion α $[1/K]$	2.05×10^{-5}

Table 4: Material properties of brass

Properties	**Aluminum**
Mass Density ρ $[kg/m^3]$	2700
Young's Modulus E $[MPa]$	72000
Poisson's Ratio μ	0.3
Thermal Expansion α $[1/K]$	2.36×10^{-5}

Table 5: Material properties of aluminum

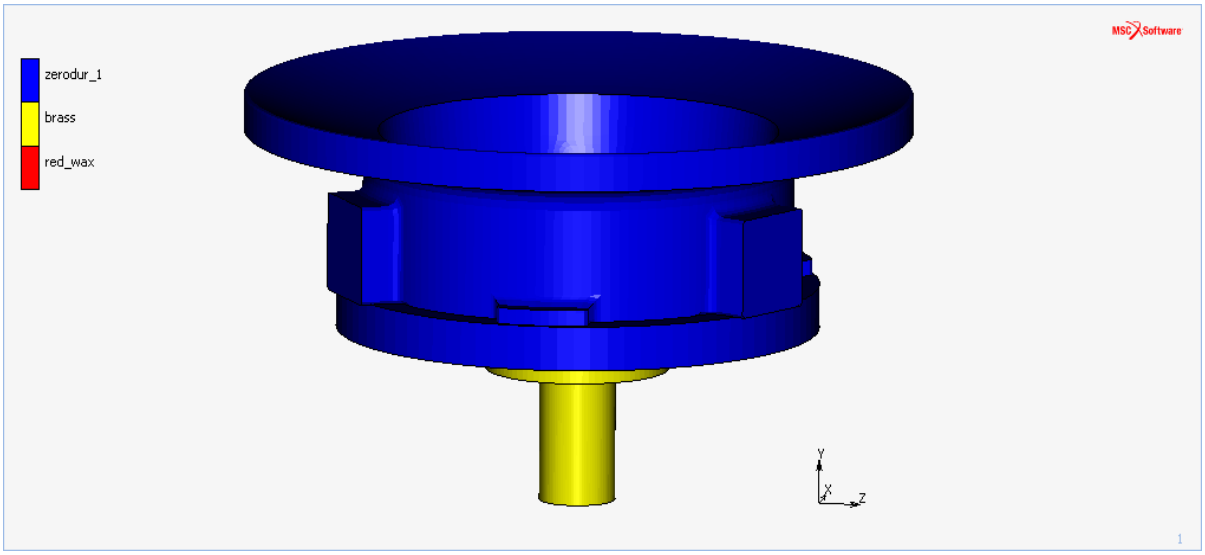

Figure 30: Assignments of materials. Blue- ZERODUR mirror and disk

A challenge in the carried work has been in determining the mechanical properties of the red wax, since there is any information from providers when is addressed to this issue. Red wax is an isotropic viscoelastic material, which is another reason of non-linearity of the process. Marc has two models that represent viscoelastic materials. First can be defined as a Kelvin-Voigt model, and the second is a general hereditary integral approach.

The Kelvin model allows the rate of change of the inelastic strain to be a function of the total stress and previous strain, while in hereditary integral model the stress-strain equations in viscoelasticity are not only dependent on the current stress and strain state, but also on the entire history of development of these states. This constitutive behavior is most readily expressed in terms of Duhamel integrals, which are formed by considering the stress or strain build-up at successive times. Two equivalent integral forms exist: the stress relaxation form and the creep function form. In MSC Marc, the stress relaxation form is used. Stress relaxation functions represent the response to a unit applied strain and have characteristic relaxation times associated with them.

We concluded that the best mechanical properties that represent red wax are as listed in the table 6.

Properties	Red Wax
Mass density ρ $[kg/m^3]$	970
Young's Modulus E $[MPa]$	1000
Poisson's Ratio μ	0.35
Thermal Expansion α $[1/K]$	1×10^{-5}
Shear Constant G $[MPa]$	110 160 100
Relaxation time t_r [s]	140 1000 200

Table 6: Material properties of red wax

The rate processes in many viscoelastic materials are known to be highly sensitive to temperature changes. Such temperature-dependent properties cannot be neglected in the presence of any appreciable temperature variation. For example, there is a large class of polymers which are adequately represented by linear viscoelastic laws at uniform temperature. These polymers exhibit an approximate translational shift of all the characteristic response functions with a change of temperature, along a logarithmic time axis. This shift occurs without a change of shape (fig. 31). These temperature-sensitive viscoelastic materials are characterized as Thermo-Rheologically Simple. Such properties for wax are given in table 7.

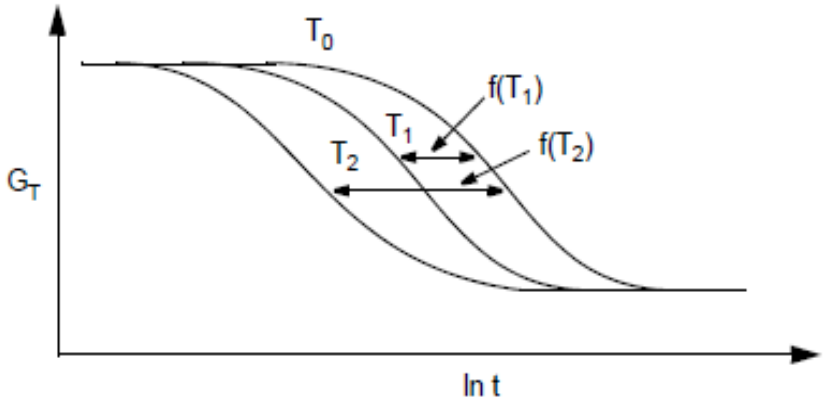

Figure 31: Relaxation Modulus vs. Time at Different Temperatures

Thermo-Rheologically Simple	
Reference temperature [℃]	45
C_1	6
C_2	101.6

Table 7: Thermo- Rehologically Simple properties for wax.

The variables $C_1, C_2,$ and T_0 come from Williams–Landel–Ferry Equation (WLF). WLF is an empirical equation associated with time–temperature superposition.

$$log_{a_T}(T) = \frac{-C_1(T - T_0)}{C_2 + (T - T_0)} \quad (10)$$

where *T* is the temperature, T_0 is a reference temperature chosen to construct the compliance master curve and C_1, C_2 are empirical constants adjusted to fit the values of the superposition parameter a_T.

6.1.3 Contact Bodies

The simulation of many physical problems requires the ability to model the contact phenomena. The analysis of contact behavior is complex because of the requirement to accurately track the motion of multiple geometric bodies, and the motion due to the interaction of these bodies after contact occurs. This includes representing the friction between surfaces and heat transfer between the bodies if required. There are two types of contact bodies in Marc – deformable and rigid. The type of contact between wax and holder is Meshed (Deformable).

Another reason why we are dealing with a non-linear process is the contact between the wax and the holder as in our simulations is described in the fig. 32.

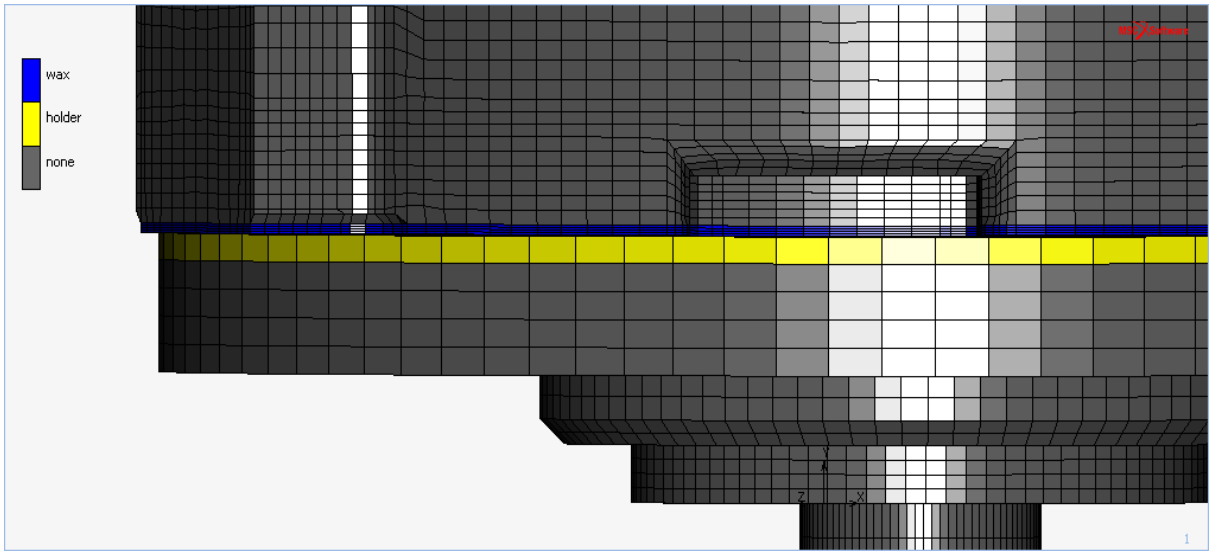

Figure 32: The contact bodies assigned for this process.

6.1.4 Initial conditions

As initial condition for this process we assigned nodal temperature at 23 ℃ for all nodes.

6.1.5 Boundary conditions

Marc is based on the stiffness method and deals primarily with force-displacement relations. In a linear elastic system, force and displacement are related through the constant stiffness of the system; the governing equation of such a system can be expressed as

$$F = Ku \tag{11}$$

which we use, where K is the stiffness matrix and, u and F are nodal displacement and nodal force vectors, respectively. Equation can be solved either for unknown displacements subjected to prescribed forces or for unknown forces (reactions) subjected to prescribed displacements. We must prescribe at least a minimum number of boundary conditions to insure that rigid body motion does not occur.

In doing so in our simulation we used two types of boundary conditions: Structural Fixed Displacement, where the holder is fixed in x, y and z direction, while the upper part of the Zerodur mirror is fixed in x, y and z direction, and

State Variable Nodal Temperature which is applied for whole geometry as is shown in the fig. 33, where we can see the steps of heating the wax up to 70℃ for 100 sec, after 600 sec starts the cooling for 3300 sec, and all the system after 4000 sec stays for 345600 sec at 23℃, which is not represented in the graph for the purpose of better visibility.

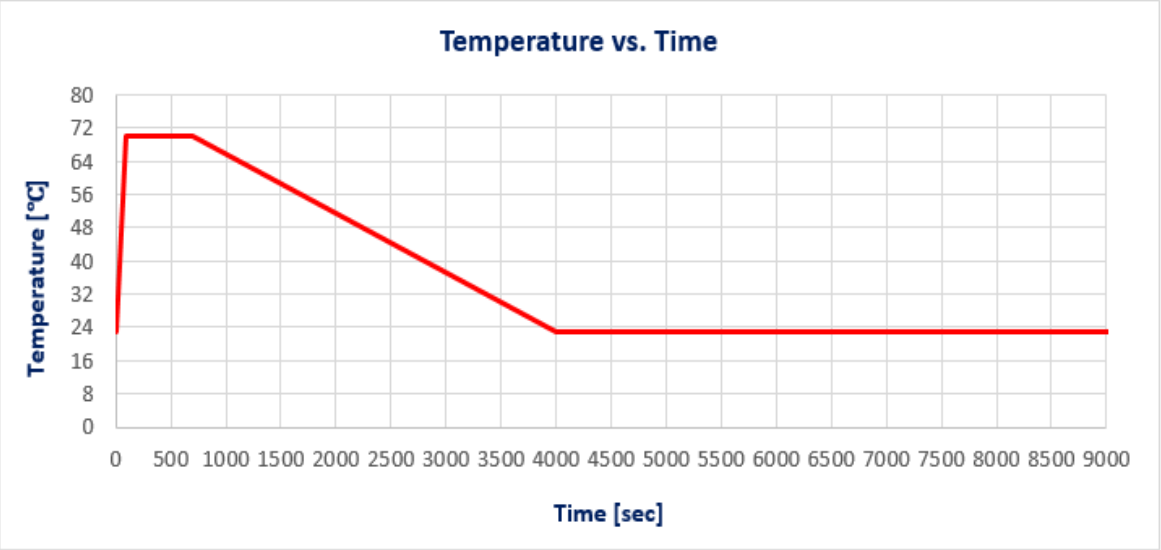

Figure 33: Nodal Temperature versus time for whole geometry

Chapter 7: Comparison of results from simulations and experiments

7.1 Results from numerical simulations

We performed numerical simulation firstly for Zerodur mirror placed on the Zerodur disk, and after that we made numerical simulations also for the case when the Zerodur mirror is placed on the aluminum disk. Based on these simulation in MSC Marc we came to conclusion that by using the Zerodur disk as our "block" where the Zerodur mirror will be glued gives less than perfect results and this we can obviously see in the figures below.

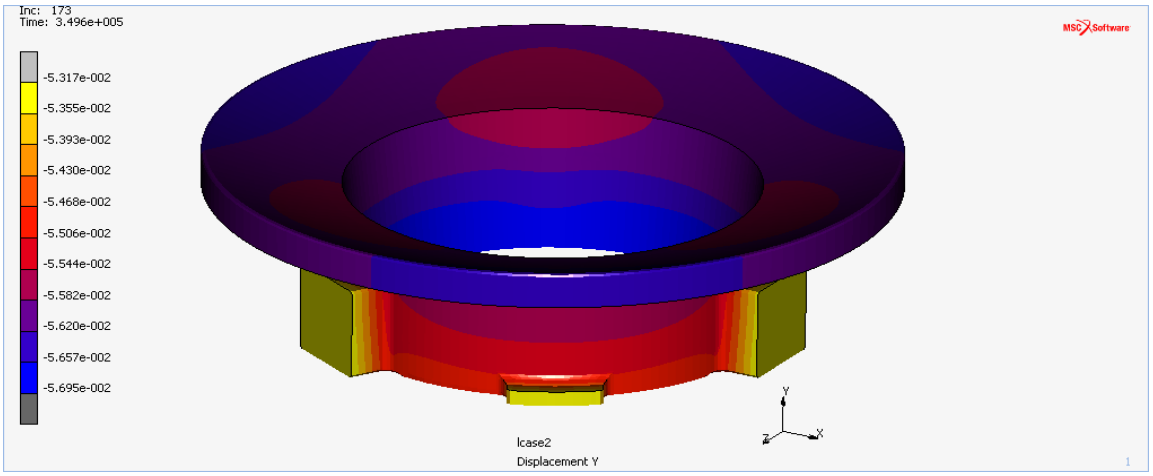

Figure 34: Displacement of Zerodur mirror on Zerodur disk

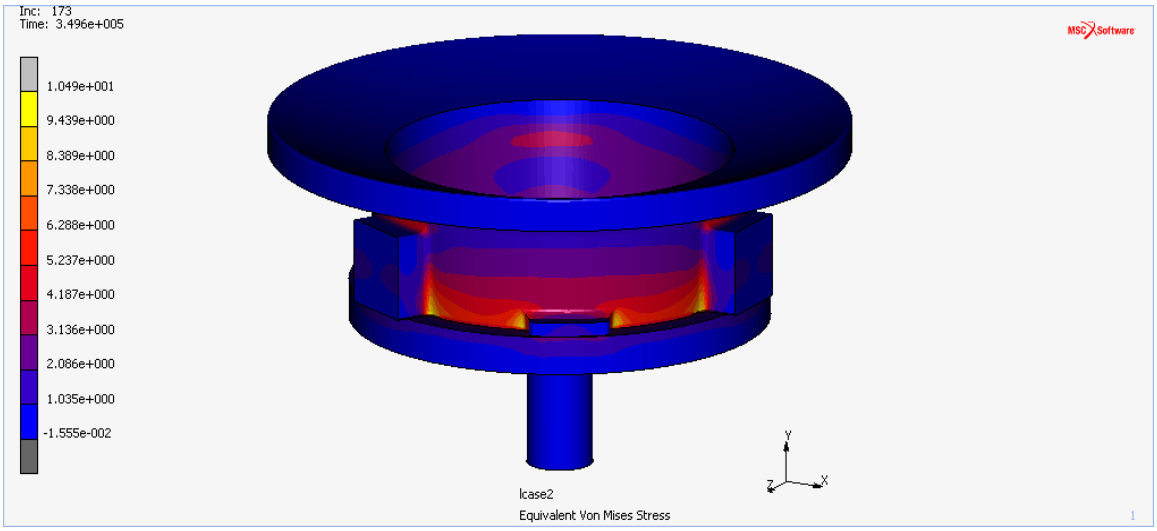

Figure 35: Equivalent Von Mises Stress for Zerodur mirror and disk

Figure 36 shows displacement of the mirror on y direction with respect to time. The graph shows the displacement of 7 nodes of the Zerodur mirror selected in same line, and for all these nodes the displacement is shown for all increments (349600 sec) in logarithmic scale, which is done for all the graphs of displacement below as well.

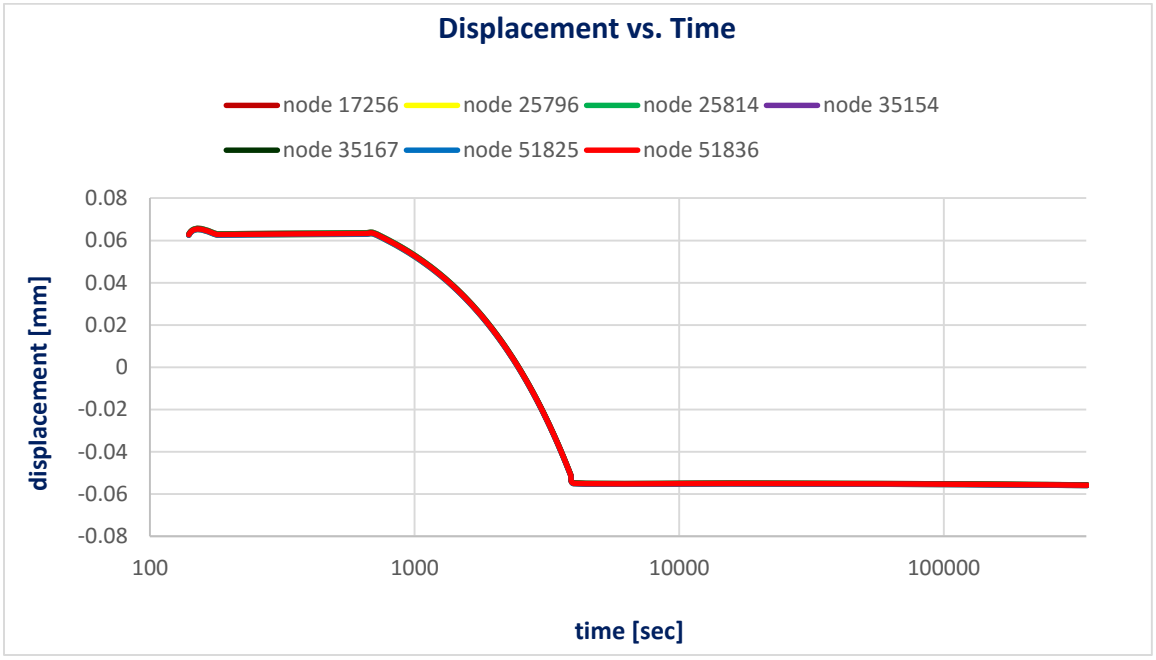

Figure 36: Displacement in y direction versus time of Zerodur mirror on Zerodur disk

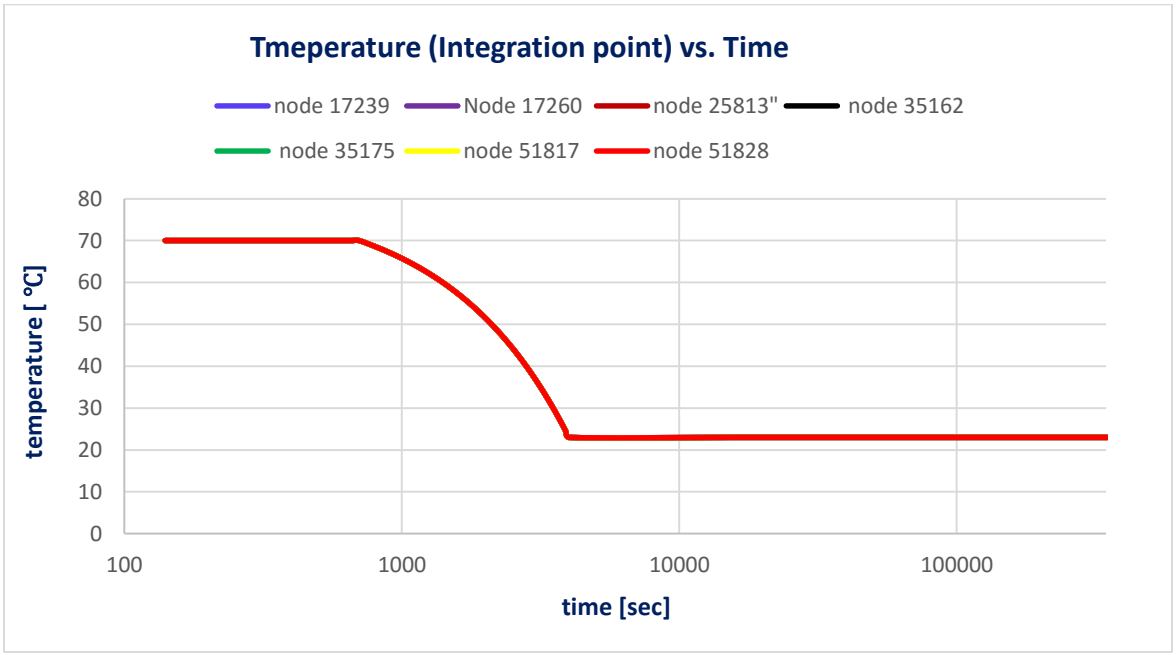

Figure 37: Temperature versus time (every 20th node picked) in the mirror placed over Zerodur disk.

In the figure 38 are represnted the equivalent von mises stres with respect to time for red wax. To show this we picekd every 20th node on the same line of mesh of the red wax. We can see form the graph that the maximum of von mises stress for the wax, 5. 96 MPa respectively is around 4000 secsonds, which is the state of the wax cooled and turned into solid phase after being melted, and when comparing these with von misses stress in figure 44 (for aluminum disk) we see when using Serodur disk equivalent von misses stress are lower.

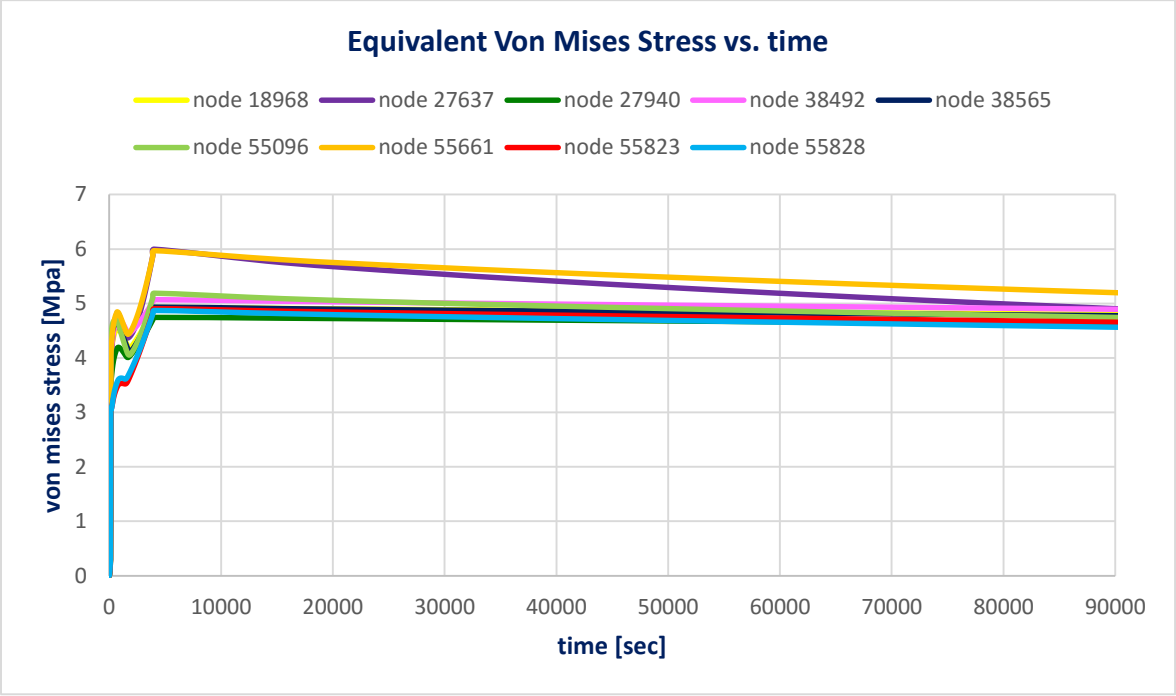

Figure 38: Equivalent Von Mises Stress vs. time of wax for wax over Zerodur disk

Equivalent von misses stresses for wax over Zerodur disk (one node picked).

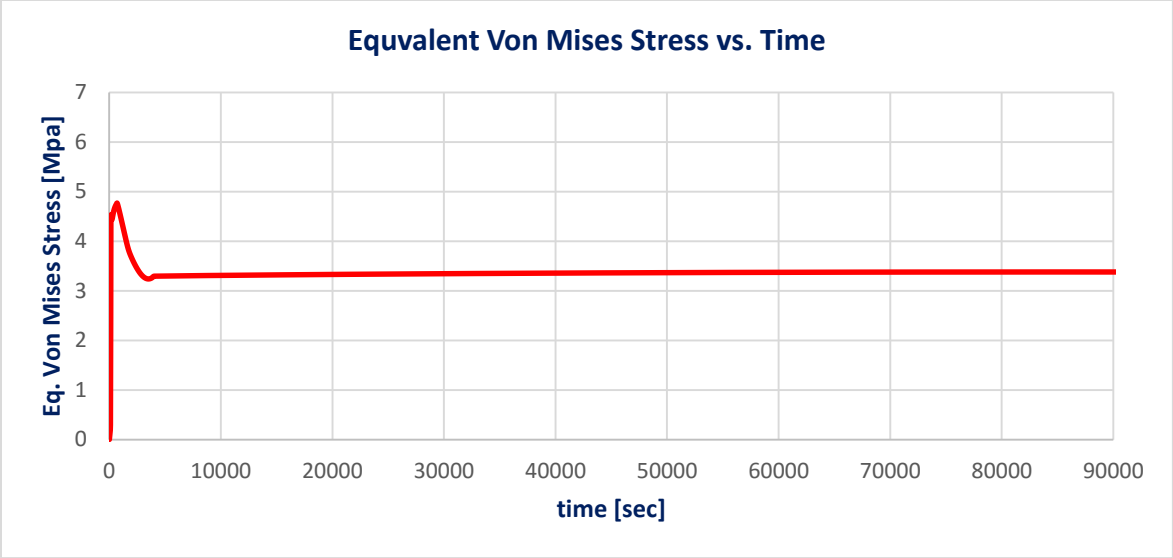

Figure 39: Equivalent Von Mises Stress versus time of ZERODUR mirror and disk

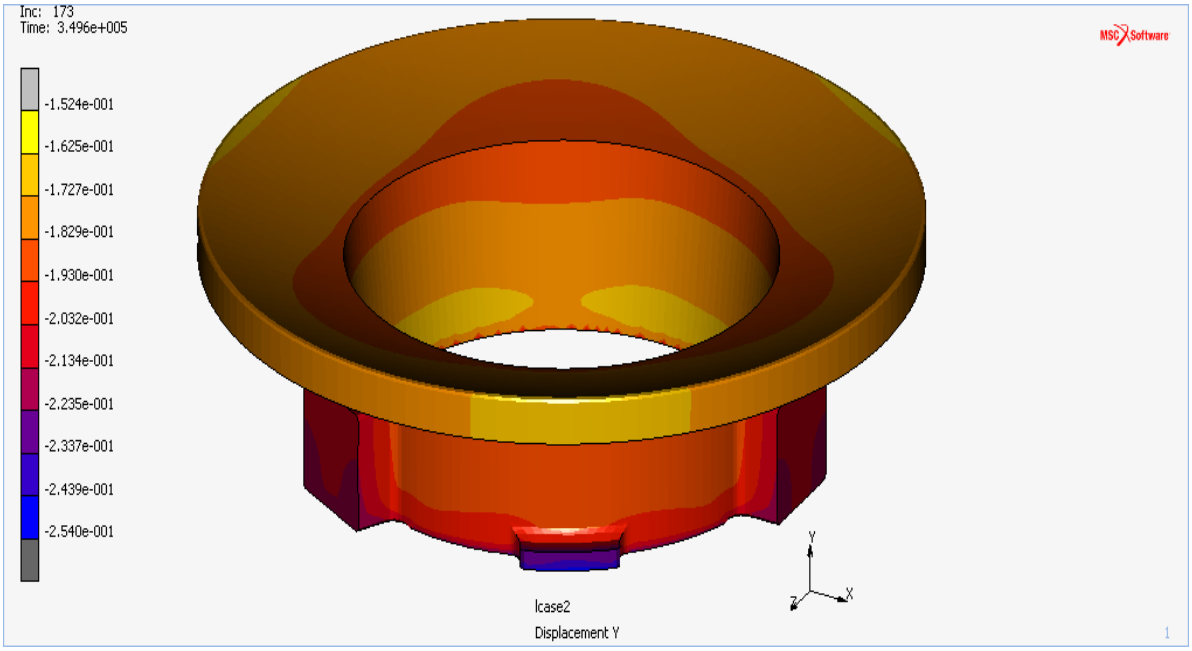

Figure 40: Displacement of Zerodur mirror on aluminum disk

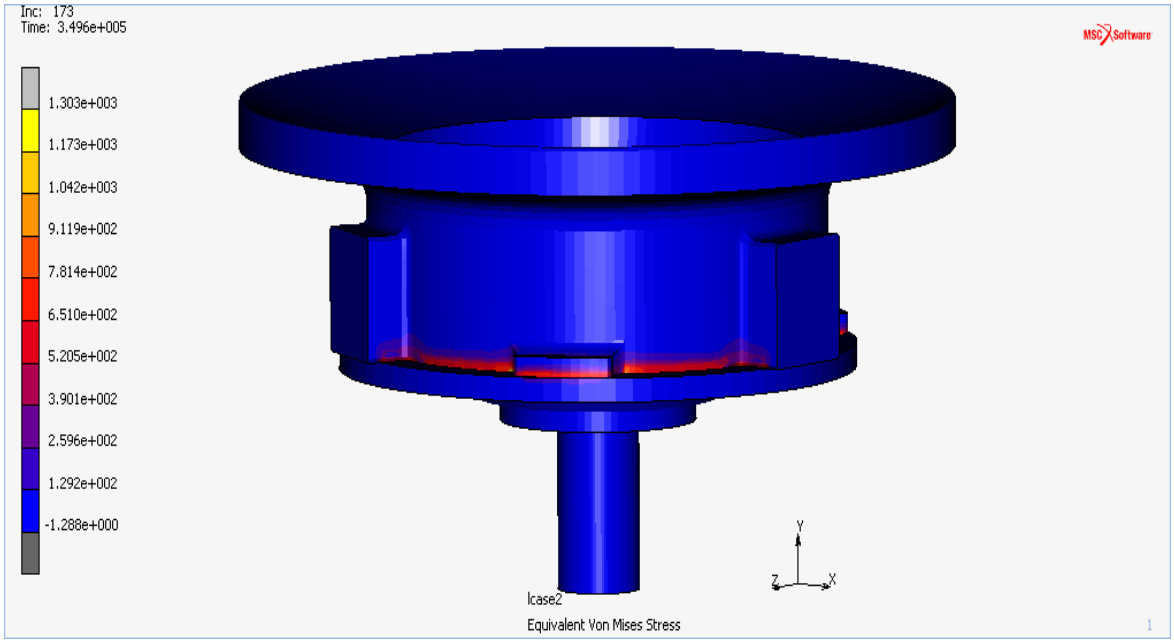

Figure 41: Equivalent Von Mises Stress of Zerodur mirror on aluminum disk

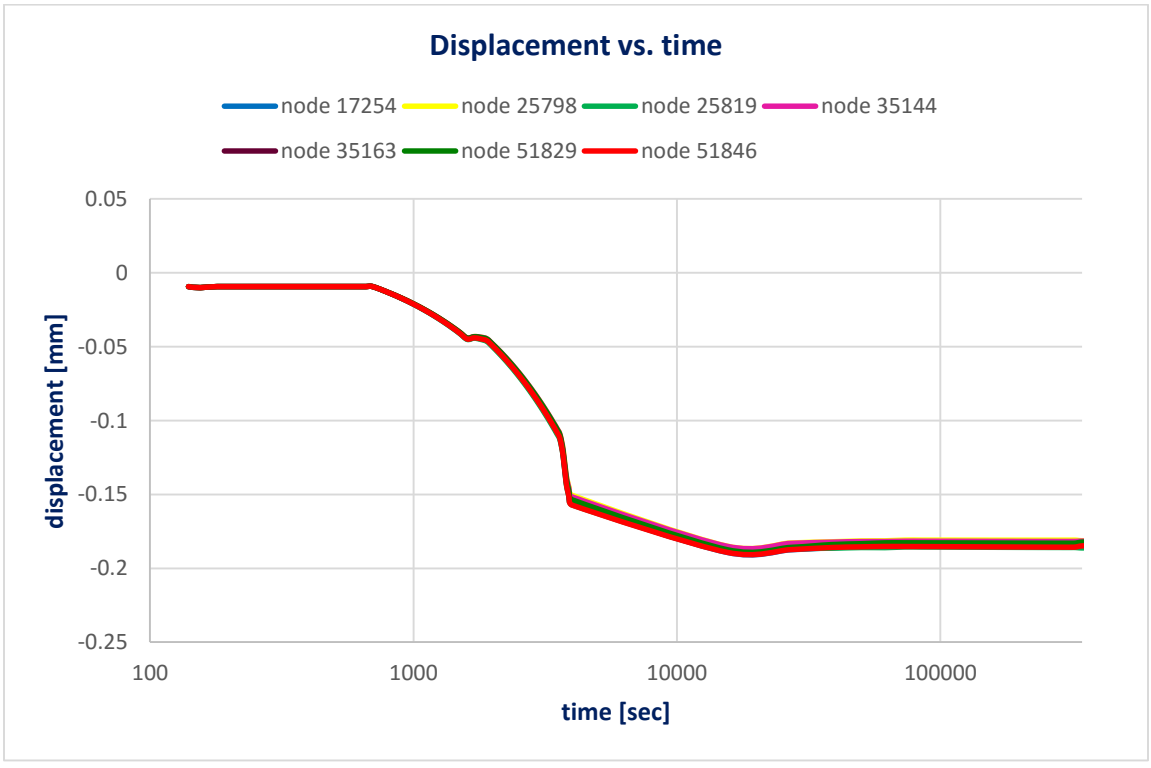

Figure 42: Displacement versus time of Zerodur mirror on aluminum disk

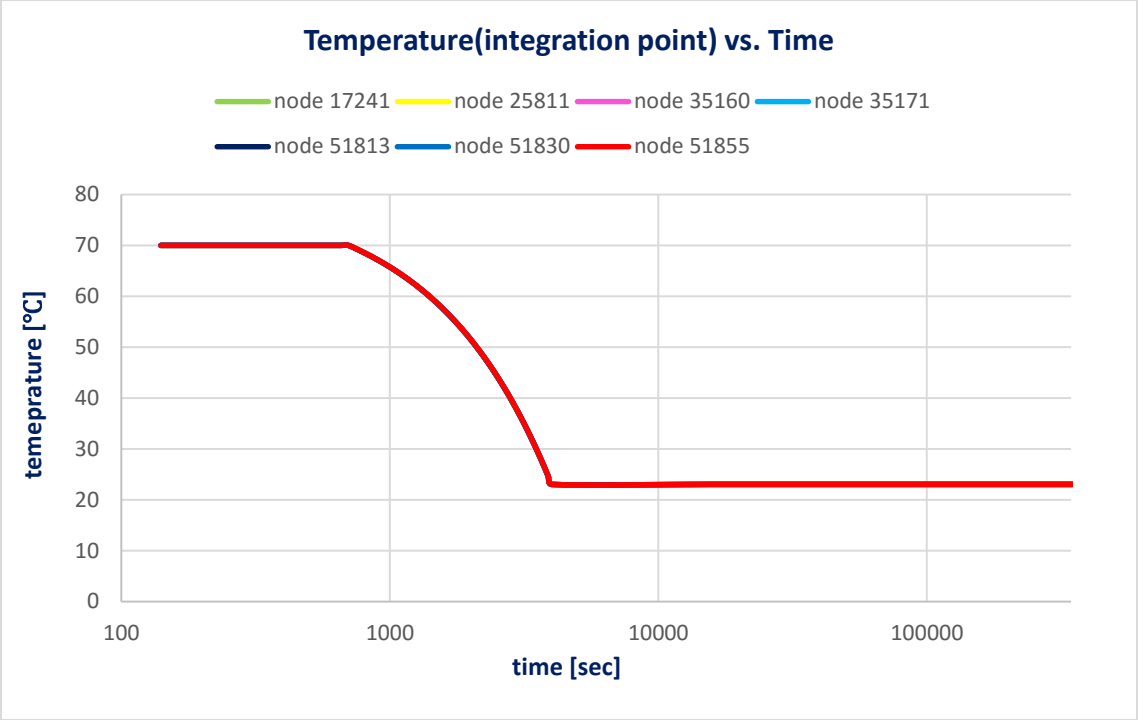

Figure 43: Temperature versus time on the mirror placed on aluminum disk (every 20th node picked)

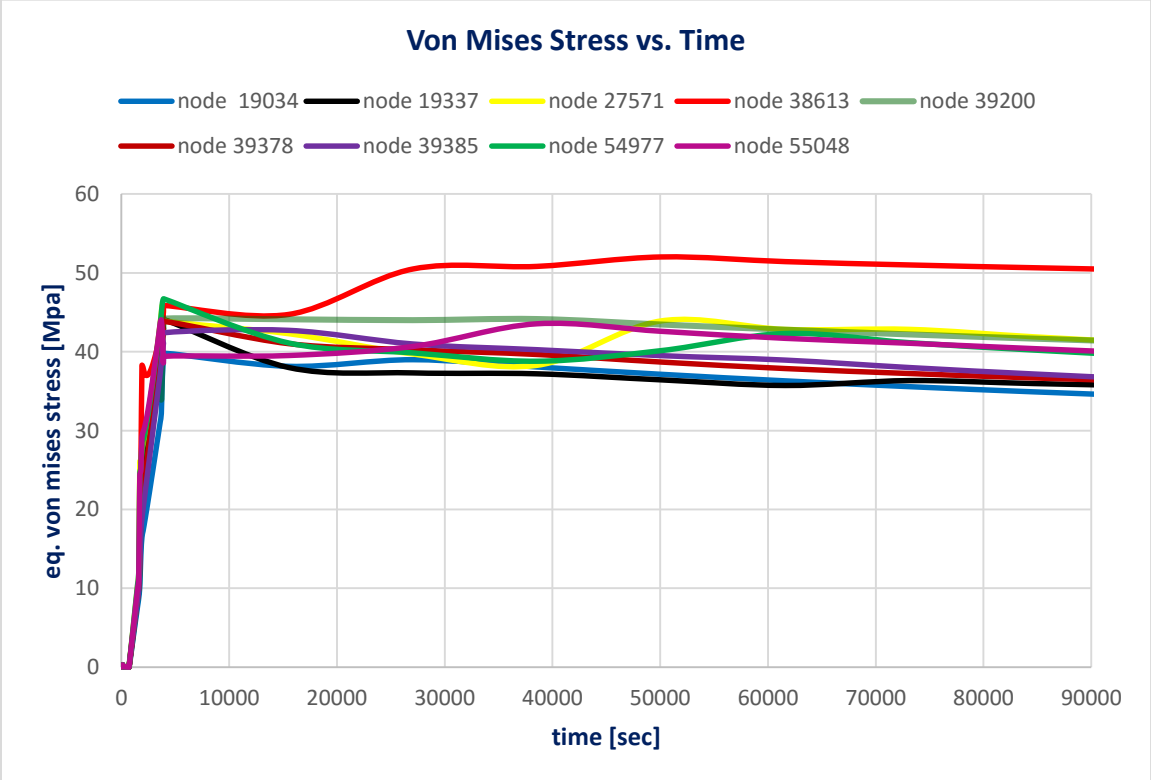

Figure 44: Equivalent Von Mises Stress for wax on aluminum disk versus time (every 20th node picked)

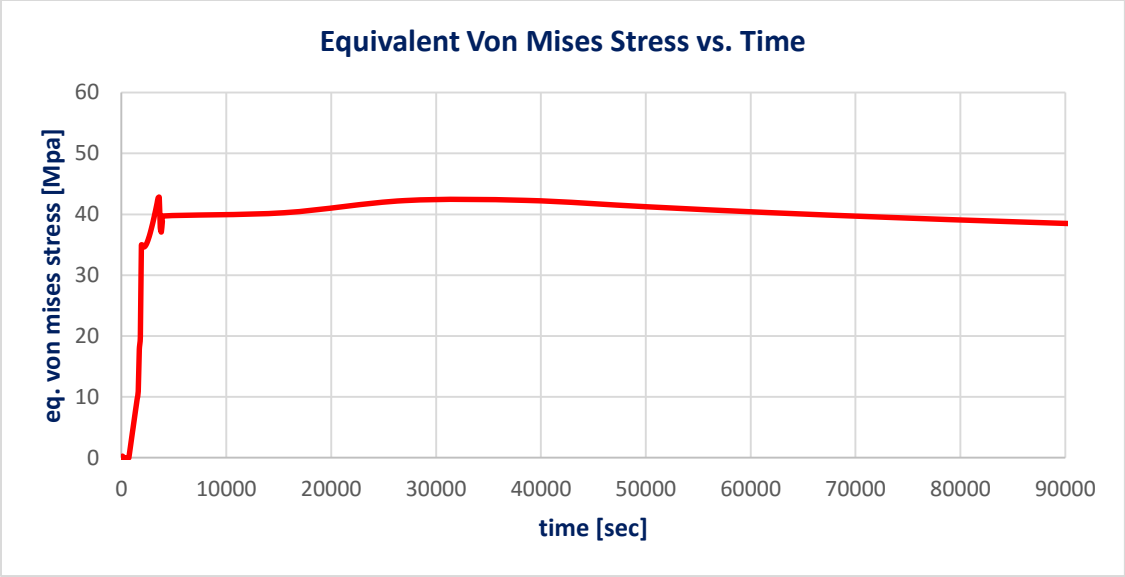

Figure 45: Equivalent Von Mises Stress versus time of red wax placed on aluminum disk (one node picked on the wax)

In fig. 46 we have shown the comparison on the displacement when we use Zerodur and aluminum disk, where we can clearly see that for the Zerodur disk displacement is lower, which fact leads us to understand that using Zerodur disk is much more better and gives a great improvement of the mirror shape.

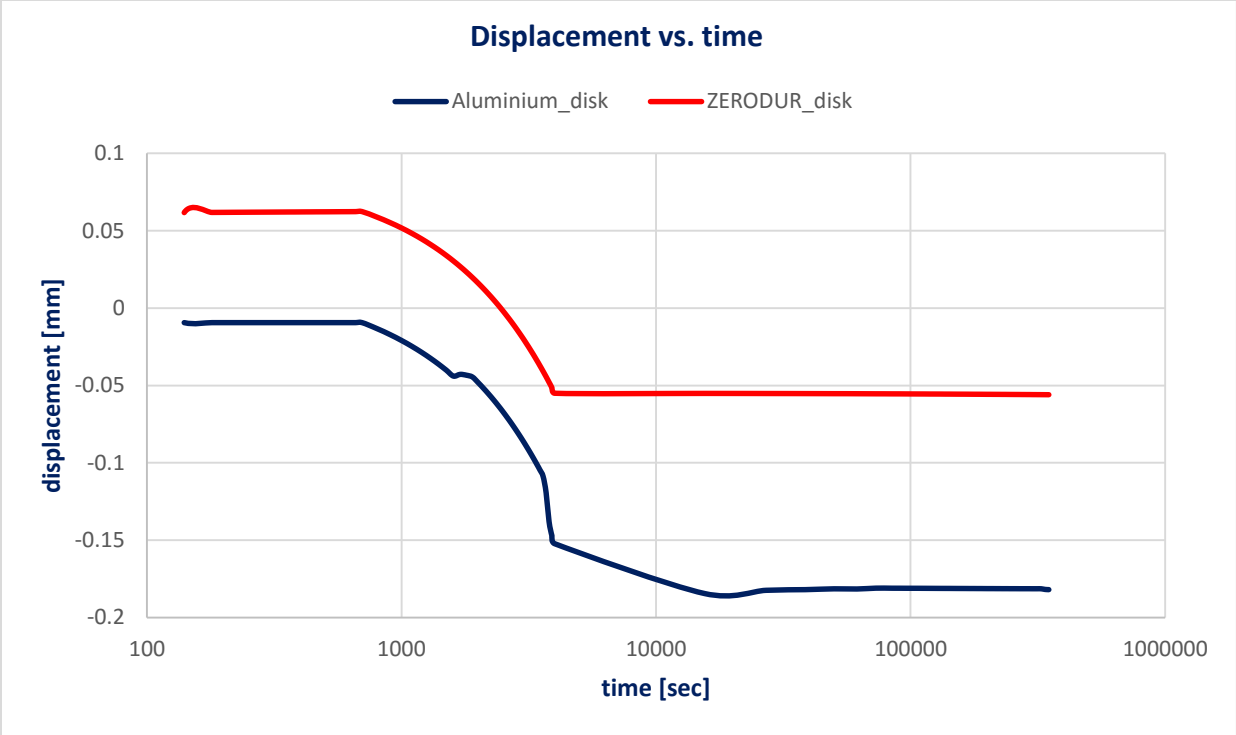

Figure 46: Displacement versus time of Zerodur mirror disk and Zerdour mirror on aluminum disk

7.2 Results from Experiments

All measurements of mirror surface topology are done by using the LuphoScan (see appendix). LuphoScan measurements are interferometric, scanning-metrology systems based on MWLI technology (multi-wavelength interferometry). They are designed to perform ultra-precision non-contact 3D form measurements mainly of rotationally symmetric surfaces such as aspheric lenses. By using LuphoScan we can measure almost every material such as transparent, specular, opaque, and ground with diameters up to 420mm.

Figure 47: LuphoSacn device

We have collected in tables all the measured data for tangential deviation (PV/RMS) for three most important cases such as:

- Material behavior
- Time depending behavior, and
- Temperature tests

and at the same time represented all of them in graphical way. For more information about how the data were gathered we put also in the appendix all the LuphoScan figures of surface topology.

Material behavior	Tangential Deviation PV/RMS $[nm]$	
	Al. holder	Zerodur holder
After Grinding	1138/174	547/56
	793/165	384/52
After ball polishing	1048/127	327/58
	370/93	123/24
After polishing in raster mode	1346/183	360/57
	517/103	138/31
After 2D shape correction	733/147	472/87
	417/100	213/37
After 3D shape correction	1083/187	248/17
	269/72	97/21
After release from the holder	4282/750	318/42
	***/463	168/37

Table 8: Tangential deviation for aluminum and Zerodur disk (unpublished results of TOPTEC) [26]

The values for tangential deviation (PV/RMS) are shown in figure 48 as well, where in an easiest way we can compare the change of mirror shape during consecutive steps of polishing for both aluminum and Zerodur disk. It is obvious that Zerodur disk leads to significant reduction of mirror shape instability.

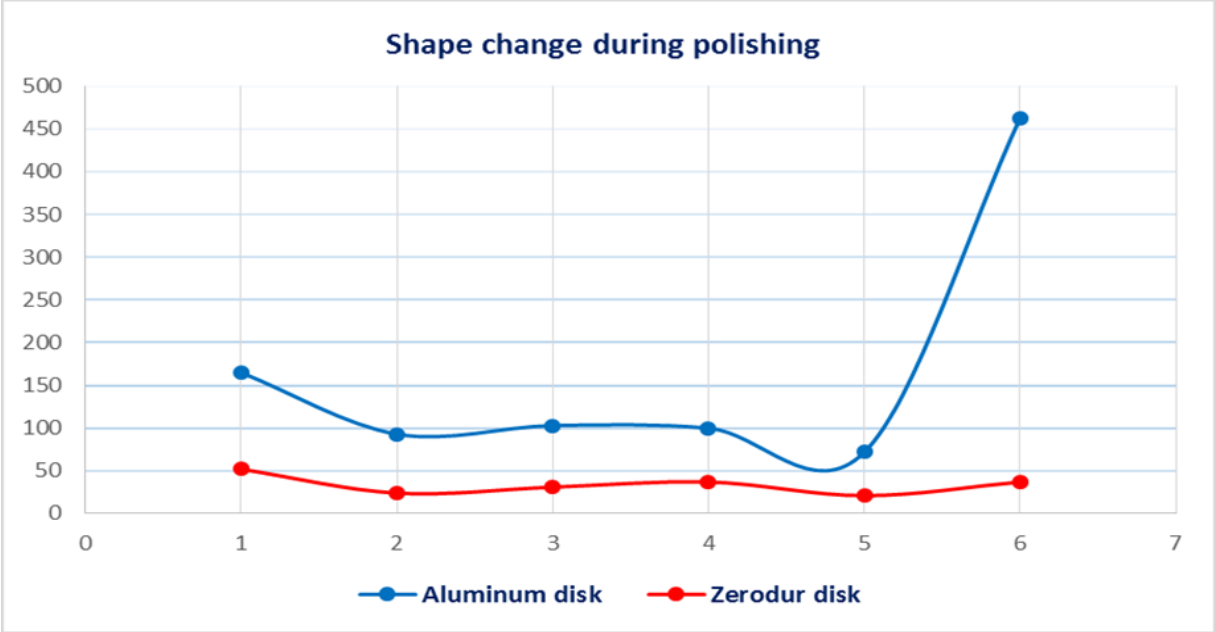

Figure 48: Material behavior (unpublished results of TOPTEC) [26]

Time depending behavior	Tangential deviation PV/RMS $[nm]$	
	PV/RMS	Time $[h]$
Shape after removing from Al disk	4429/947	0
Shape after cementing on Zerodur disk	4748/976	193
Shape after tempering in shape generator	4732/978	56
After tempering in shape generator +2h in lab.	4740/978	4
After grinding	4606/236	48
One day after grinding	4804/230	24

Table 9: Tangential deviation for consecutive steps of manufacturing of the mirror (unpublished results of TOPTEC) [26]

In this graph is shown time depending behavior of mirror shape and we can conclude that Zerodur disk leads to the great improvement in the process quality.

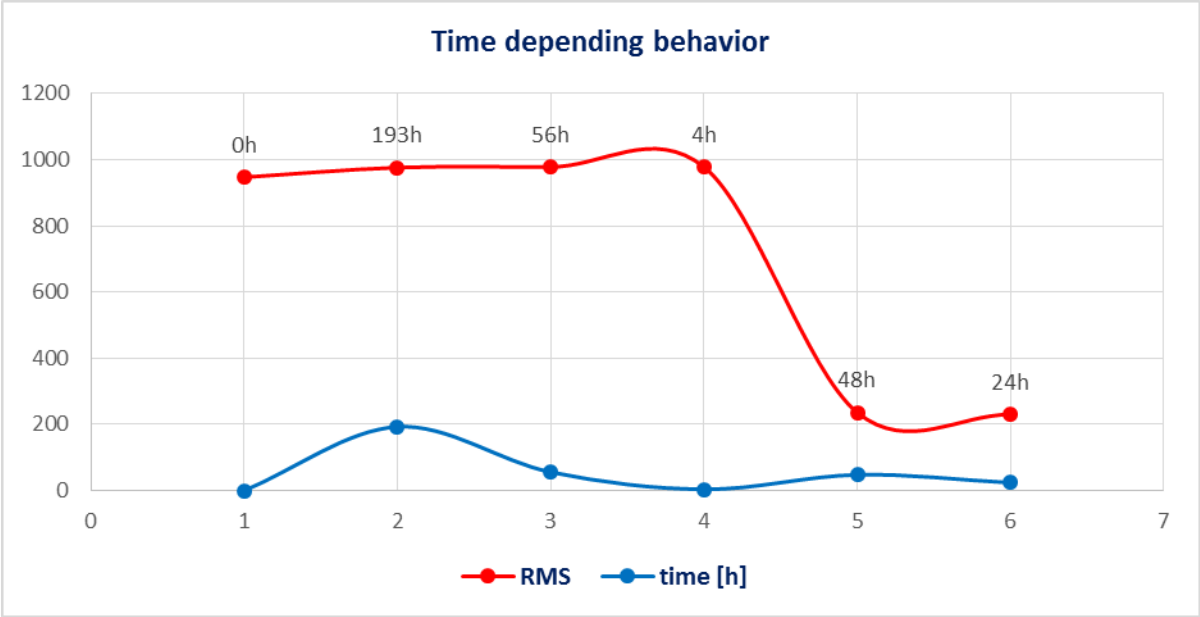

Figure 49: Graph of time depending behavior of mirror (unpublished results of TOPTEC) [26]

Temperature tests of aluminum holder shows that the influence of the temperature is small in this process.

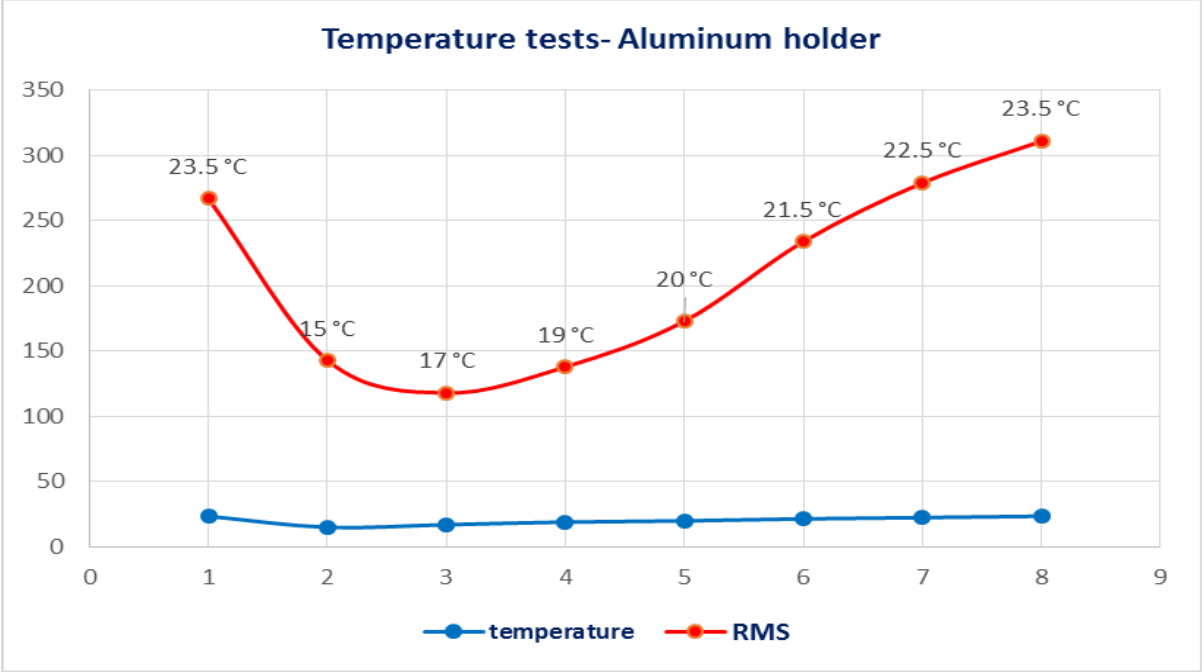

Figure 50: Graph of temperature tests of aluminum (unpublished results of TOPTEC) [26]

Chapter 8: Conclusion

After getting results from numerical simulations in MSC Marc for cases of using Zerodur and aluminum disk which is presented in this work we came in conclusion that using of Zerodur disk leads to great improvements in the quality of process. The effect of the temperature is small.

The conclusion from the FEM model we tested with experiments also, where we see for respective steps of grinding and polishing that using Zerodur disk gives significant reduction of shape instability. Using of aluminum disk is the standard way. However, it failed in this case. So it was necessary to find the solution – which was the Zerodur disk.

With experiments we also came in conclusion that temperature effects are small.

Even though we got good results from setting our values, further work in this field is suggested in testing more viscoelastic properties of wax adhesive with both FEM tool and experiments as well,

References

[1] P. Shore, Machining of Optical Surfaces in Brittle Materials, Cranfield: Cranfield University, 1995.

[2] P. Psota , V. Ledl , P. Vojtisek , R. Dolecek and V. Kopecky, "3D form inspection of grinded optical surfaces by digital holography," *Proceedings of SPIE - The International Society for Optical Engineering*, Vols. Proc. of SPIE Vol. 9442 944218-1, January 2015.

[3] J. O. Lofken , "Pushing the limits with Extreme Ultraviolet Light," *Innovation 20,* pp. 30-33, 2008.

[4] S. J. Taylor , G. E. Sommargren, D. W. Sweeney and R. M. Hudyma, "The Fabrication and Testing of Optics for EUV Projection Lithography," *American Society for Precission Engineering 13th Annual Meeting ,* 1998.

[5] K. Kemp and S. Wurm, "EUV lithography," *Comptes Rendus Physique 7,* pp. 875-886, 2006.

[6] E. Verroi, V. Da Deppo , G. Naletto, S. Fineschi and E. Antonucci, "METIS- ESA Solar Orbiter Mission Internal Straylight Analysis," *International Conference on Space Optics*, no. ICSO , 2014.

[7] ESA/SRE, "Solar Orbiter- Exploring the Sun-heliosphereconnection," ESA, June 2011.

[8] S. Cesare, " METIS design overview and technical challenges," 2012.

[9] X. Tonnellier, "Precision Grinding for Rapid Manufacturing of Large Optics," Cranfield University, 2008-2009, p. 236.

[10] E. Heynacher, "Aspharichе Optik- Warum sie gefordert und wie sie gefertigt wird," *Seeis Informationen ,* Vols. Vol. 24, pp., no. Carl Zeiss. Oberkochen , p. Heft 88, 1978-79.

[11] P. Schellekens , N. Rosielle, E. Vermeulen, M. Vermeluen and W. Pril, "Design for Precision: Current Trends," *Annals of CRIP,* vol. Vol. 47/2, 1998.

[12] P. Shore, "ULTRA PRECISION SURFACES," Ultra Precision and Structured Surfaces Centre, Cranfield University Precision, Wales, Cranfield, UK , 2008.

[13] I. F. Stowers, R. Komanduri and E. Baird, "Review of precision surface generating processes and their potential application to the fabrication of large optical components," *Proceedings of the SPIE,* Vols. Vol. 966, pp., pp. 62-73., 1998.

[14] B. Braunecker, R. Hentschel and H. J. Ti, Advanced Optics Using Aspherical Elements, Bellingham, Washnington USA: SPIE, 2007.

[15] H. Shinno , "Ultraprecision," *The International Academy for Production Engineering* , Vols. DOI 10, 1007/978-3-642-20167-7., 2014.

[16] "Advances in Precsion Grinding," Tata McGraw-Hill Publishing Company Limited, 2007.

[17] E. Brinksmeier, C. Heinzel and M. Wittman, "Friction, Cooling and Lubrication in Grinding," *CRIP Annals- Manufacturing Technology* , vol. Volume 48, no. Issue 2, p. 581–598, 1999.

[18] D. Anderson and J. Burge, "Optical Fabrication," in *The Handbook of Optical Engineering* .

[19] S. AG, "ZERODUR- Zeor expansion glass cearmic," SCHOTT AG, 2011.

[20] M. Software, Marc 2014, Volume A: Theory and User Information, 2014.

[21] B. Zhang, , J. Wang, , F. Yang, and Z. Zhu, , "The effect of machine stiffness on," *International Journal of Machine Tools & Manufacture*, 1999.

[22] T. Vit, R. Melich, J. Vaclavik and V. Ledl, "Design of Precise Lightweight Mirror," *Applied Mechanics and Materials,* Vols. 284-287, pp. 2717-2722 , 2013.

[23] Y. Yamamoto, H. Suzuki, T. MORIWAK and T. OKINO, "DEVELOPMENT OF CROSS AND PARALLEL MODE GRINDING MACHINE FOR HIGH NA ASPHERICAL MOLD AND DIE," Shinagawa, Tokyo, JAPAN , 2006.

[24] T. Hobson , "Ultra precision technologies," AMETEK, 2016.

[25] F. Twyman , "Non Spehrical Surfaces," in *Prism and Lens Making* , 1952, p. Chapter 10.

[26] František Procháska, "Development of grinding and polishing process of the Zerodur mirrors, "unpublished results, IPP TOPTEC 2015-2016".